

# 1 SEATANI: hazards from seamounts in SouthEast Asia, Taiwan, 2 and Andaman and Nicobar Islands (eastern India)

3 Andrea Verolino<sup>1</sup>, Su Fen Wee<sup>2</sup>, Susanna F. Jenkins<sup>1,2</sup>, Fidel Costa<sup>1,2,3</sup>, Adam D. Switzer<sup>1,2</sup>

4  
5 <sup>1</sup>Earth Observatory of Singapore, Nanyang Technological University, 50 Nanyang Ave, Singapore, 639798,  
6 Singapore

7 <sup>2</sup>Asian School of Environment, Nanyang Technological University, 50 Nanyang Ave, Singapore, 639798,  
8 Singapore

9 <sup>3</sup>Institut de Physique du Globe de Paris, Université Paris Cite, CNRS, 1 Rue Jussieu, Paris, 75005, France

10  
11 Correspondence to: Andrea Verolino

12 Email: andrea.verolino@ntu.edu.sg

13  
14 **Abstract.** Submarine volcanism makes up approximately 85% of volcanism taking place on Earth, and its  
15 eruptions have the potential to cause several hazards, including ash dispersal, pumice rafts, pyroclastic density  
16 currents, sector collapses and tsunamis. Recent examples include the eruptions in Japan and in the Kingdom of  
17 Tonga in 2021 and 2022 respectively, but there has been little to no study of submarine volcanism in Southeast  
18 Asia and its surroundings. Here we provide a compilation of 466 seamounts from the region, from different  
19 published sources, through the SEATANI dataset (Southeast Asia + Taiwan + Andaman & Nicobar Islands). We  
20 use this newly compiled dataset to assess on a regional level the seamount hazard potential and exposure potential  
21 as a springboard for future more quantitative hazard studies for the region. The hazard potential was assessed  
22 through seamount morphological/structural analyses, to determine the seamount evolution stage and, grade of  
23 maturity. The exposure potential was evaluated with two different approaches: An areal analysis of the number  
24 of assets within a 100 km radius of each seamount; and the development of a hazard-weighted seamount density  
25 map to highlight potential areas of interest for future more-in-depth studies. Our results show that there are several  
26 potentially hazardous seamounts in this region, and Taiwan had the highest hazard and exposure potential, for all  
27 assets considered, while Philippines, Indonesia and Vietnam have relatively high exposure potential for submarine  
28 communication cables and ship traffic density. The results from this work serve as a first step for Southeast Asian  
29 and neighbouring countries to become more resilient against and prepared for submarine volcanic eruptions in the  
30 region.

## 31 **1 Introduction**

32 Volcanic seamounts are submerged or mostly submerged volcanoes, and can be defined as “*any geographically*  
33 *isolated topographic feature on the seafloor taller than 100 m, including ones whose summit regions may*  
34 *temporarily emerge above sea level*” (Staudigel et al., 2010). The number of volcanic seamounts around the world  
35 is in the order of tens of thousands. A recent estimate suggests that there are ~35,000 seamounts >400-m in height  
36 (Gevorgian et al., 2023); however, limitations in detection suggest that this is a significant underestimate,  
37 especially in shallow continental shelf regions close to land masses (Kim and Wessel, 2011). Volcanic seamounts  
38 are generally detected through satellite-derived altimetry and gravimetry, however, these methods are limited by

39 resolution (i.e. kilometric scale, not allowing for the detection of small seamounts), and noise in the gravimetry  
40 measurements in areas with thick sequences of sediments (e.g. within continental margins; Kim and Wessel,  
41 2011). It is likely that there are many more seamounts globally than those we are aware of.

42 Volcanic seamounts, particularly deep-sea ones, have been traditionally considered to be a negligible threat to  
43 society (Cas, 1992; Whelley et al., 2015), for several reasons. The first is that most of them are completely  
44 underwater, hence they are economically and logistically difficult to monitor, map and sample compared to their  
45 subaerial counterparts; as a result, their eruption frequency and intensity have not been properly assessed. A  
46 second reason is that they are often located far from major landmasses, hence not considered an imminent threat  
47 to populations. Thirdly, most of them have their summit in deep waters (> 3000 m b.s.l.), and this makes them  
48 hypothetically less hazardous than shallower volcanoes, because of the high hydrostatic pressure hindering  
49 explosivity. Finally, most ocean intraplate volcanoes, particularly those approaching subduction zones, are likely  
50 to be extinct and have not been active for millions of years (Staudigel and Clague, 2010), hence, have been not  
51 considered of interest for volcanic hazard. As a result, seamounts are vastly understudied around the world. In  
52 January 2022, the eruption of Hunga volcano in the SW Pacific (Kingdom of Tonga), demonstrated that erupting  
53 seamounts can have a large impact on people and their activities, even in a remote location such as the southwest  
54 Pacific Ocean. The eruption produced the highest volcanic plume ever recorded (~58 km) (Taha et al., 2022),  
55 unusually fast tsunamis that travelled across the Pacific Ocean for thousands of kilometres (Gusman et al., 2022),  
56 and damage of millions of USD across the entire region, with the Kingdom of Tonga being the most affected  
57 (damage equivalent to ~19% of the national GDP, and several casualties recorded) (The World Bank, 2022).

58 A few notable seamounts around the world have been studied in detail using multibeam surveys to obtain high  
59 resolution bathymetry (up to 1-m), and in a few cases were accompanied by sampling and/or video recording of  
60 the eruptions from Remotely Operated Vehicles (ROV's). Typically, these investigations occur after an impactful  
61 eruption. Examples include Havre volcano, (Kermadec arc), NW Rota-1 (Mariana arc), West Mata (Tonga arc),  
62 Fani Maoré (NW of Madagascar), Axial caldera (Juan de Fuca ridge) (Carey et al., 2014; Murch et al., 2019a;  
63 Dürig et al., 2020; Embley et al., 2006; Chadwick et al., 2008; Schnur et al., 2017; Clague et al., 2011; Dziak et  
64 al., 2015; Murch et al., 2022; Feuillet et al., 2021; Hammond, 1990; Caress et al., 2012; Clague et al., 2013),  
65 (Carey et al., 2014; Murch et al., 2019a; Dürig et al., 2020; Embley et al., 2006; Chadwick et al., 2008; Schnur et  
66 al., 2017; Clague et al., 2011; Dziak et al., 2015; Murch et al., 2022; Hammond, 1990; Caress et al., 2012; Clague et  
67 al., 2013; in the Kermadec arc (north of New Zealand), which erupted in 2012 and produced what is considered  
68 one of the largest submarine silicic eruptions ever recorded (Carey et al., 2014; Murch et al., 2019a; Dürig et al.,  
69 2020); NW Rota 1 in the Mariana arc (Embley et al., 2006; Chadwick et al., 2008; Schnur et al., 2017), and West  
70 Mata in the Tonga arc (Clague et al., 2011; Dziak et al., 2015; Murch et al., 2022), which produced medium-  
71 intensity Strombolian explosions and lava flows (both eruptions were recorded); Fani Maoré volcano, offshore  
72 Mayotte island (NW of Madagascar), which was formed between 2018 and 2019, growing more than 800 m from  
73 the seafloor, and erupting both explosive and effusive products, despite being mostly basanitic in composition  
74 (Feuillet et al., 2021); Axial caldera, on the Juan de Fuca ridge (offshore of California, USA), which produced  
75 several effusive basaltic eruptions in recent years (last eruption in 2015), but also has evidence of past large  
76 explosive eruptions (Hammond, 1990; Caress et al., 2012; Clague et al., 2013), among others. All the above-  
77 mentioned submarine volcanoes were surveyed as part of large, well-funded, multidisciplinary projects that  
78 provided a wealth of data (bathymetry, rock geochemistry, tephra granulometry and componentry, etc.). It is

79 logistically impossible to apply the same approaches to the thousands of seamounts worldwide, therefore, a  
80 regional approach is needed to characterise seamounts in a simple and efficient manner that allows for a broad  
81 focus on lesser-known areas potentially at risk.

82 Past global studies on volcanic seamounts have included classifications based on morphology or growth stage  
83 of the edifice (Schmidt et al., 2000; Wessel, 2007; Staudigel and Clague, 2010; Kim and Wessel, 2011; Gevorgian  
84 et al., 2023). Some authors found direct relationships between seamount morphometric parameters (e.g. basal  
85 width and height) and linked them to the tectonic setting (Schmidt et al., 2000; Gevorgian et al., 2023). These  
86 classifications, however, have never been used for assessing hazard potential or exposure on a regional scale.

87 For the region of Southeast Asia (SEA), there has been some effort in assessing hazards from what we define  
88 here as volcanic seamounts; examples include Krakatau and Banua Wuhu, Indonesia, and Didicas, Philippines  
89 (Hamzah et al., 2000; Paris et al., 2014; Mutaqin et al., 2019; Hidayat et al., 2020; Zorn et al., 2022; NCEI/WDS,  
90 n.d.), however, these studies focused on volcanic islands, and there is little or no consideration for the hazard  
91 potential from fully submerged volcanoes.

92 Our newly compiled dataset includes 466 seamounts from different sources (Fig. 1, Table S1 – Supplementary  
93 information) and enclosed within three (Indonesia, Philippines and Vietnam) of the nine Exclusive Economic  
94 Zones (EEZs) of Southeast Asia (Brunei, Burma, Cambodia, Indonesia, Malaysia, Philippines, Singapore,  
95 Thailand and Vietnam) and the neighbouring countries Taiwan and eastern India (Andaman and Nicobar Islands),  
96 and has been named SEATANI (**SEA + Taiwan + Andaman & Nicobar Islands**). This dataset includes both fully  
97 submerged volcanoes and some small volcanic islands, whose submerged portion makes up most of the edifice.

98 This region is interesting for several reasons: (i) It is very volcanologically active, but little is known about its  
99 underwater features; (ii) Millions of people live along its coasts; (iii) There are infrastructure worth billions of  
100 dollars on the seafloor of the target area (e.g. submarine telecommunication cables) (Wang et al., 2019); and (iv)  
101 It has a rather high density of ship traffic. Based on thisIn this paper, we have two main goals: one is to characterise  
102 the seamount morphology and evolution stage and link them to the *hazard potential* for seamounts in the region,  
103 and the other is to highlight areas of high *exposure potential*, to motivate and focus future studies. To accomplish  
104 the first goal of characterising seamounts and assess their hazard potential, we conduct qualitative (seamount type:  
105 caldera, guyot, simple cone, composite cone) and quantitative morphological analysis (height, summit water  
106 depth) by using open-access bathymetry datasets (e.g. Gebco 2021; NOAA DEM Global Mosaic; NOAA  
107 Multibeam Bathymetry Mosaic). Additionally, we also conducted a more qualitative analysis based on higher  
108 resolution bathymetry (Multibeam data from NOAA – 90m/pixel), where we highlight key seamount features  
109 (e.g. submarine landslides, explosive craters, new seamounts) that otherwise would not be detected from Gebco  
110 or the NOAA DEM Global mosaic dataset. Despite the multibeam data having limited regional coverage (< 10%),  
111 they reveal significant seafloor morphologies that can motivate future quantitative hazard assessments for the  
112 region, e.g. numerical hazard modelling. The second goal of highlighting areas of high exposure potential is  
113 achieved through two types of analysis, a quantitative one, where the number of assets and activities (population,  
114 submarine fibre-optic cables, and ship traffic density) within 100 km of volcanic seamounts is counted; and a  
115 semi-quantitative one, where the hazard potential of each seamount is used to weight the potential areal hazard  
116 extent for the entire region of interest. We acknowledge that our work has some limitations, in particular, the  
117 hazard and exposure potential are not quantified based on geological, geochemical, tectonic setting, age, and  
118 frequency/magnitude information, which are indeed needed for more quantitative studies (a focused discussion is

119 provided later in the text to address these points). However, our intent with this work is to provide the basic but  
120 fundamental elements for future more quantitative studies.

121 **2 Methods**

122 **2.1 Compilation of SEATANI**

123 Following the seamount definition from Staudigel et al. (2010), here only used for volcanic seamounts, we pre-  
124 compiled a list of seamounts for the region of interest by using three different types of sources: 1) The GVP  
125 database (Global Volcanism Program 2013), where we include seamounts that have erupted from the Pleistocene  
126 (n= 42); 2) The seamount dataset Gevorgian et al. (2023) (n= 405), which is an updated version of the dataset  
127 from Kim and Wessel (2011), where they used statistical methods to differentiate volcanic from non-volcanic  
128 seamounts; and 3) Seamounts from individual studies around the southeast Asian region found in literature (n= 129  
130 35) (Li et al., 2013; Fan et al., 2017), which have been detected through geophysical methods (i.e. interpretation  
131 of seismic profiles), for a total of 482 entries for the region considered. The definition proposed by Staudigel and  
132 colleagues, however, does not provide specific directions on islands (at what extent a volcanic island is still  
133 considered a seamount). Therefore, in order to guarantee reproducibility and to maintain our broad focus on the  
134 unknown hazard potential of seamounts, we did not include islands whose emerged volume was > 30% of the  
135 total seamount volume, and/or their maximum elevation was > 1000 m above sea level (a.s.l.) (more details on  
136 this methodology are provided in the supplementary information). Following this criterion, none of the seamounts  
137 from the Gevorgian et al. (2023) dataset or from the literature studies were removed, however, 16 GVP volcanoes  
138 were excluded (Table S2, Supplementary information), bringing the total to 466 volcanic seamounts. Despite the  
139 choice of 30% and 1000 m a.s.l. was somewhat arbitrary, it allows comparisons across studies and is in line with  
140 our focus here, which is primarily on submarine volcanoes.

141 **2.2 Bathymetry and exposure datasets**

142 For the bathymetry, we used different datasets of different resolution based on each specific purpose. namely  
143 These include *Gebco 2021, DEM global mosaic* (from NOAA/NCEI), and *Multibeam Bathymetry Mosaic* (from  
144 NOAA/NCEI). Gebco 2021 is a gridded bathymetric dataset with interval grid of 15 arc-second (450-m/pixel),  
145 and was used for the quantitative morphological classification (seamount growth stages) and exposure potential  
146 analyses (quantitative and semi-quantitative). Despite the relatively low/medium resolution, it has global coverage  
147 with bathymetry data deriving from different acquisition methods (Fig. S1, supplementary material), and was  
148 clipped for the region of interest (North: 36.5°, South: -14.3°, West: 82.0°, East: 145.6°). The DEM global mosaic  
149 is a colour shaded relief raster file that was exclusively used for the qualitative morphological classification  
150 (seamount morphotypes); it is a seamless bathymetry/topography mosaic that combines DEMs from several  
151 sources (e.g. direct and indirect measurements from ships and satellites) and different resolutions (450-m/pixel or  
152 better), with the higher-resolution DEMs displayed on top of the lower resolution ones (where both available).  
153 Since DEMs of different resolution cannot be extrapolated from this file, but must be downloaded individually,  
154 we used the mosaic format for efficiency and for visualization purposes only. The file was clipped with the same  
155 extent as Gebco 2021, for consistency. The Multibeam Bathymetry Mosaic is the dataset with the highest  
156 resolution among the datasets used here (90-m/pixel); it is a gridded colour shaded relief, deriving from multibeam  
157 survey data collected over the years (from ~1980 to present). This dataset has a coverage lower than 10% for the  
158 region of interest, therefore was only used for qualitative image analyses, both for the morphological classification

159 (in combination with the DEM Global mosaic) and for the characterization of bathymetric features (see  
160 discussion) at some of the locations enclosed within our study area (where there was data coverage).

161

162 To assess the exposure potential, we used different open-access datasets for population, submarine  
163 communication cables and ship traffic density. We chose these assets for three reasons: (i) Data were available  
164 for quantitative analyses on GIS environment on a regional scale; (ii) We considered them as the assets potentially  
165 more exposed to multiple hazards from a submarine volcanic eruption in a regional perspective (e.g. air traffic  
166 exposure was not quantified here because potentially only exposed to development of a tephra column); And (iii)  
167 such exposure assessment from submarine volcanic eruptions has not been done before, particularly for submarine  
168 communication cables and ship traffic density, which instead have shown to be vulnerable elements to natural  
169 hazards (Ohno et al., 2022; Speidel, 2022). For population estimates, we used LandScan (Sims et al., 2022), which  
170 has a spatial resolution of around 1 km (30 arc-seconds) and has been widely used in previous volcanic hazard  
171 assessments (Reyes-Hardy et al., 2021; Jenkins et al., 2022; Verolino et al., 2022a). For the submarine cables we  
172 used data from *TeleGeography* (last update in 2017); while for the ship traffic density we utilised data from *The*  
173 *World Bank Group*, which reports hourly Automatic Identification Systems (AIS) positions, recorded between  
174 January 2015 and February 2021, at a spatial resolution of 500-m/pixel. This dataset included separate files for  
175 commercial, leisure, passenger, oil and gas, and fishing vessels respectively, however, we used the combined file,  
176 assuming no distinction across vessel types.

177

### 178 **2.3 Volcanic seamounts classification**

179 Volcanic seamounts were classified through two different approaches: 1) Qualitative, based on seamount shape  
180 (i.e. caldera, guyot, simple cone, composite edifice; Fig. 2 and Table 2); and 2) Quantitative, based on the  
181 seamount height and depth that gives a stage of growth, as proposed by Staudigel and Clague (2010) (Stage 1 to  
182 5: defined in Table 3). Both classifications were obtained from analyses conducted in GIS environment (Esri®  
183 ArcMap 10.7.1). For the qualitative classification, we overlaid the seamount locations over the bathymetry  
184 datasets, and conducted visual image analysis to establish morphotype (Table 2, Fig. 2), using the highest  
185 resolution available for that area (NOAA DEM Global Mosaic, 450-m resolution or better, or NOAA Multibeam  
186 data, 90-m resolution). This morphological assessment was conducted by authors A. Verolino and S.F. Wee, to  
187 ~~verify test for~~ consistency and reproducibility, as the classification can be partially subjective. For the quantitative  
188 method, we applied the Staudigel and Clague (2010) classification (used here for the first time for hazard  
189 purposes) and obtained the seamount maximum summit height and base water depth within a 30 x 30 km bounding  
190 box of the given seamount location (following Kim and Wessel, 2011). These were in turn used to assign a stage  
191 of growth. Staudigel and Clague (2010) also included Stage 6 seamounts (those approaching the trench of a  
192 subduction zone, or that already started being subducted), however, to maintain the growth stage classification in  
193 a state that is as quantitative as possible, we included them within the low hazard potential i.e. Stage 1, 2 or 5  
194 seamounts (i.e. deep-water or extinct seamounts). We did this depending on their height and water depth though  
195 we know that the Staudigel and Clague (2010) classification, is not specific on how close to the subduction trench  
196 a seamount must be to be considered stage 6, leaving some subjectivity in the classification). We used both  
197 qualitative and quantitative classification approaches in parallel to obtain different types of information  
198 (morphological and growth stage); however, for exposure calculation we refer only to the quantitative approach  
199 (i.e. growth stage).

200  
201 **2.4 Exposure analysis**

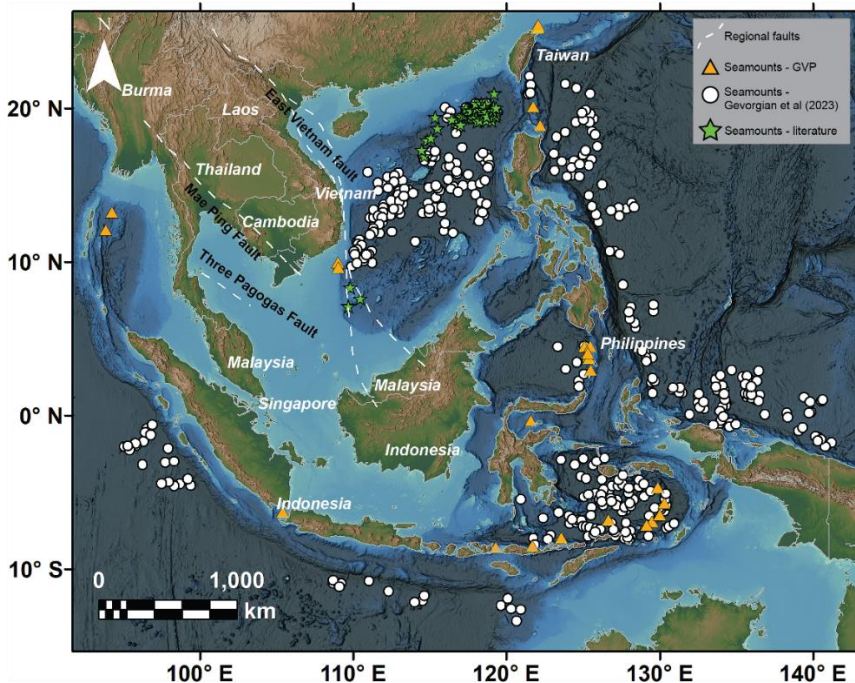
202 We conducted two types of exposure potential assessments: 1) A quantitative analysis of population, submarine  
203 communication cables and ship traffic density within 100 km from each seamount; and 2) A semi-quantitative  
204 assessment, through a hazard-weighted seamount density map, to assess what countries are more likely to be  
205 threatened by a seamount within the study region.

206 For the first type of assessment, we chose concentric 100 km radii to include exposure potential of the above-  
207 mentioned assets with the approximation that this would include the more damaging processes from most volcanic  
208 hazards (e.g. tephra fallout, PDCs, sector collapses). This choice is in line with previous regional volcanic threat  
209 studies (Small and Naumann, 2001; Brown et al., 2015), however, we acknowledge that using concentric radii is  
210 an oversimplification of volcanic hazard extents (Jenkins et al., 2022).

211 The semi-quantitative assessment considered the concentration of seamounts, weighted by their hazard rank  
212 (Table 1), and highlights regions of higher hazard potential. We created a weighted seamount density map (Kernel  
213 Density Estimation, KDE), based on the seamount stage of growth, with the assumption that more heavily  
214 weighted seamounts have a greater hazard potential. The KDE was performed on Esri® ArcMap 10.7.1, which  
215 assigns a default bandwidth in function of the input dataset (~630 km in this case), and proven to be reliable in  
216 previous exposure studies (Verolino et al., 2022a). To verify whether the default bandwidth was suitable to our  
217 case, we conducted additional KDEs by manually assigning different bandwidths (named “search radius” in  
218 ArcMap) in the range 800-100 km respectively; the results, reported in the supplementary material (Fig. S2),  
219 support our choice to use the default bandwidth. The choice of weight assigned to each growth stage (Table 1)  
220 was based on the Global Historical Tsunami Database (NCEI/WDS), where out of 164 historical volcanic  
221 tsunamis (from 1610 BC to present), 115 were from volcanic seamounts; of these, 78% (n= 90) were from stage  
222 4, 20% (n= 23) from stage 3, and nearly 2% (n= 2) from stage 1, 2, 3 or 5 seamounts (depth of seamount unknown).  
223 To compensate the paucity of historical information/data from stages 3, 2, 1 and 5 (shallow or deep), compared  
224 to stage 4 seamounts (partially emerged), and to include volcanic hazards as well, we arbitrarily adjusted these  
225 percentages to 60% and 35% for stage 4 and stage 3 respectively, and the rest was distributed through stage 1, 2  
226 and 5 seamounts (Table 1). Exposure potential was then assessed based on the extent of high-density area (higher  
227 exposure potential:  $> 2.9 \times 10^{-6}$  seamounts/km<sup>2</sup>) obtained from the KDE.

228  
229  
230 **Table 1. Seamount hazard ranking based on the Global Historical Tsunami**  
231 **Database (NCEI/WDS) and growth stage from Staudigel and Clague (2010).**

Seamount hazard ranking	Seamount growth stage	Historical volcanic tsunami occurrence (%)	Hazard weight
1	4	78	0.6
2	3	20	0.35
3	2	2	0.03
4	1		0.01
5	5		0.01



233  
234  
235

Figure 1. Map of the study area with seamounts locations and major regional faults.  
Basemap is from NOAA (DEM Global Mosaic).

236 **3 Linking seamounts morphology and evolution stage with their potential hazards**

237 **3.1 Seamount morphotype**

238 Seamount morphology [can be used to infer information](#) about the seamount eruptive history. An important  
239 consideration is that once seamounts are completely submerged, they do not experience major erosion, retaining  
240 most of their original morphological constructive features, unless new eruptions and/or disruptive events such as  
241 landslides take place. Therefore, classifying seamounts based on their large-scale morphological features  
242 overcomes the resolution issue that we generally have at smaller scales. Below in Table 2 (examples shown in  
243 Fig. 2), we provide general guidelines [we](#) used for the classification of seamount morphotypes. A background for  
244 each morphotype, with a link to their hazard potential and with relevant examples from the literature, is provided  
245 in the supplementary information file.

246  
247

**Table 2. Seamount morphotype descriptions.**

Seamount morphotype	Description
Simple Cone	Regular-shaped and conical pointy volcanic edifice with only one vent
Composite edifice	Irregularly shaped volcanic edifice with one or more vents. This morphotype also includes ridges and flank ephemeral cones (e.g. subaqueous portion of a volcanic island)
Caldera	Volcanic edifice with prominent central depression with diameter ~ 4-8 km
Guyot	Flat-topped volcanic edifice with relatively steep flanks

248  
249  
250  
251  
252

**3.2 Seamount growth stage**

Staudigel and Clague (2010) classified seamounts based on their growth stage (Stage 1 to 5), here we use the same approach to first assign a growth stage to the SEATANI seamounts, and then link the growth stage to a given potential hazard(s) that may be common for that particular growth stage. In Table 3 we report the main

253 characteristics for each growth stage (from Staudigel and Clague, 2010), and associated potential hazards (Murch  
 254 et al., 2019a; Paris et al., 2014; Clague et al., 1990; Harders et al., 2014; Verolino et al., 2018, 2019, 2022b;  
 255 Jutzeler et al., 2014; Deardorff et al., 2011; Omira et al., 2016; Newland et al., 2022). A more comprehensive  
 256 analysis of seamount growth stages and their potential hazards is provided in the supplementary information file.

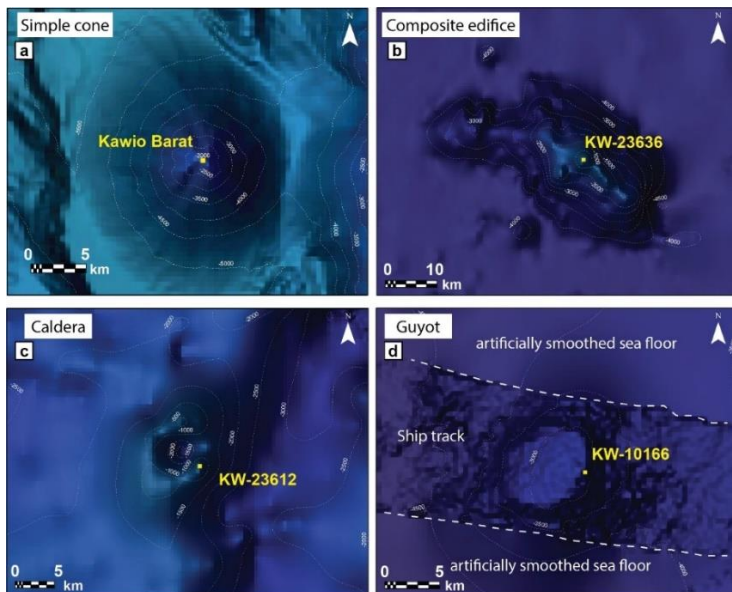
257  
 258 **Table 3. Seamount growth stage and associated potential hazards. Adapted from Staudigel and Clague (2010).**

Seamount growth stage	Description (from Staudigel and Clague, 2010))	Potential hazards (see references in the text)
1	<ul style="list-style-type: none"> <li>Seamounts 100-1000 m high and &gt; 700 m <u>below sea level</u> (b.s.l.)</li> <li>&gt; 80% lavas and &lt; 20% pyroclastic deposits</li> </ul>	<ul style="list-style-type: none"> <li>Lava flows</li> <li>Obstacles for navigation (submarines)</li> </ul>
2	<ul style="list-style-type: none"> <li>Seamounts &gt; 1000 m high and &gt; 700 m b.s.l.</li> <li>&gt; 80% lavas and &lt; 20% pyroclastic deposits</li> <li>Developed shallow magma plumbing system (especially the larger ones), potentially leading to flank instability</li> </ul>	<ul style="list-style-type: none"> <li>Lava flows</li> <li>Subaqueous eruption-fed density currents</li> <li>Subaqueous eruption column</li> <li>Pumice rafts</li> <li>Large gas bubbles</li> <li>Sector collapse</li> <li>Tsunamis</li> <li>Obstacles for navigation (submarines)</li> </ul>
3	<ul style="list-style-type: none"> <li>Seamounts &lt; 700 m b.s.l.</li> <li>&gt; 60% pyroclastic deposits</li> <li>+/- Developed shallow plumbing system (depending on seamount size)</li> <li>Higher flank instability due to abundance of pyroclastic material making up the seamount</li> </ul>	<ul style="list-style-type: none"> <li>Lava flows</li> <li>Subaqueous eruption-fed density currents</li> <li>Subaerial PDCs</li> <li>Subaqueous and subaerial eruption column</li> <li>Pumice rafts</li> <li>Sector collapse</li> <li>Tsunamis</li> <li>Obstacles for navigation (submarines)</li> </ul>
4	<ul style="list-style-type: none"> <li>Emerged seamounts (&gt; 70 vol% submerged)</li> <li>&gt; 60% pyroclastic deposits</li> <li>+/- Developed shallow plumbing system (depending on seamount size)</li> <li>High flank instability due to abundance of pyroclastic material making up the seamount</li> </ul>	<ul style="list-style-type: none"> <li>Lava flows</li> <li>Subaqueous eruption-fed density currents</li> <li>Subaerial PDCs</li> <li>Subaerial eruption column</li> <li>Sector collapse</li> <li>Tsunamis</li> </ul>
5	<ul style="list-style-type: none"> <li>Flat-topped seamounts (guyots)</li> <li>Originally emerged seamounts drowned below sea level for erosion and subsidence, and cessation of volcanic activity</li> </ul>	<ul style="list-style-type: none"> <li>Obstacles for navigation (submarines)</li> </ul>

260 **4 Results**

261 **4.1 Seamount morphology and growth stage**

262 Seamounts in our study were classified based on their morphotype (simple cone, composite edifice, caldera, guyot; Fig. 2, Table 2) and growth stage (Stage 1 to stage 5; Table 3). Results for their abundance, distribution and 264 exposure analyses are reported below (Figs. 3-6).



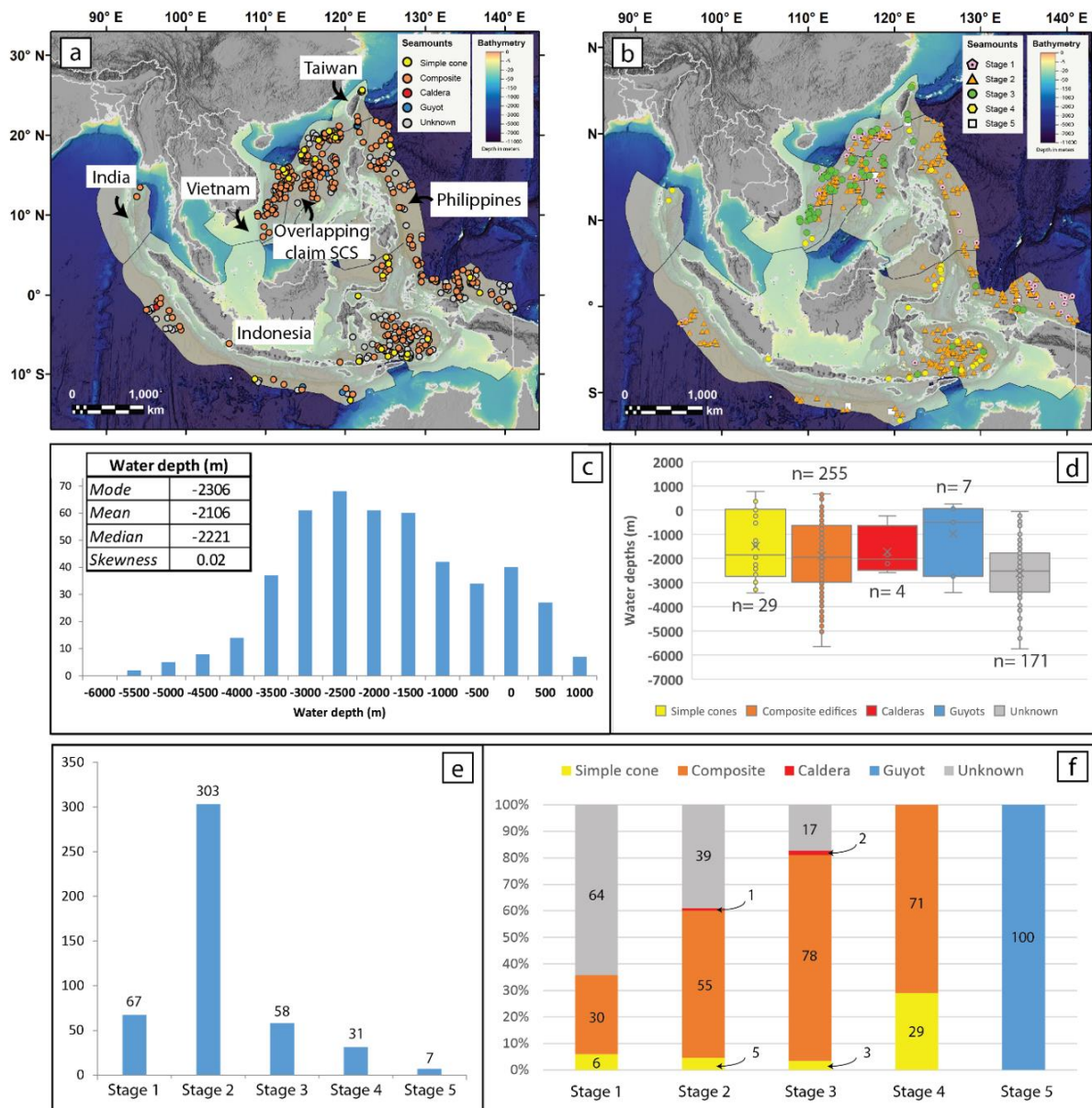
265  
266 **Figure 2. Seamount morphotype examples. Note how the seafloor appears smoothed away from ship**  
267 **track measurements due to low density of data points (d). The basemap shown here is from NOAA**  
268 **(DEM Global Mosaic).**

269  
270 Of the 466 seamounts in our catalogue, we were able to classify 295 (63%) of them into the four morphotypes; 271 the remaining 171 (37%) seamounts were not classifiable due to low resolution bathymetry data and/or because 272 they were too small. The seamounts are dominated by *composite* edifices (n= 255, 54.7%), followed by *simple* 273 *cones* (n= 29, 6.2%), and *guyots* (n= 7, 1.5%). The morphotype least represented is *calderas*, with only 4 of them 274 (0.9%). Water depths range from -5739 m b.s.l. (seamount KW-22106 of unknown morphotype; Lat: 13.81°, Lon: 275 125.58°) to 776 m a.s.l. (Paluweh, simple cone; Lat: -8.32°, Lon: 121.71°), with a *mode* of 2306 m b.s.l., *mean* - 276 2106 m b.s.l., *median* -2221, and *skewness*= 0.02 (close to symmetric distribution) (Fig. 3c). Water depths within 277 each morphotype category are relatively variable (Fig. 3d). Simple cones, composite edifices and calderas have a 278 median of about 2000 m b.s.l., while guyots are mostly closer to sea level (median ~500 m b.s.l.), and unclassified 279 seamounts cover the entire underwater range (~ 0-5700 m b.s.l.). Despite having a general broad range of water 280 depths, all the classified seamounts are also represented at relatively shallow water depths (shallow than 1000 281 m b.s.l.), and this has important implications in terms of volcanic hazard (discussed in later sections). We found 282 no particular geographic or tectonic setting distribution associated with each morphotype (Fig. 3a).

283 Results from the growth stage analysis (Fig. 3e) show that the majority of the seamounts in the study region 284 are in their *stage 2* (65%, n= 303), > 1000 m high and > 700 m b.s.l., followed by the shorter but still deep *stage* 285 *1* (14%, n= 67), shallower *stage 3* (12%, n= 58), and emerged *stage 4* (7%, n= 31) seamounts. Only 7 seamounts 286 (2%) represent *stage 5*, *flat-topped seamounts*. When comparing morphotype and growth stage distributions (Fig. 287 3f), simple cones and composite edifices are found in all growth stages, except for stage 5 (by definition), with 288 composite edifices dominating across all stages. Calderas are only found within stage 2 (1%) and stage 3 (2%)

289 seamounts, however, when a caldera complex has new cones formed within them or on their rims, we classified  
 290 them as composite edifices (e.g. Krakatau, Indonesia). Undefined seamounts dominate stage 1, however, they  
 291 decrease in percentage towards higher stages seamounts. In terms of geographic/tectonic setting, stage 1 and 2  
 292 seamounts dominate extensional and/or intraplate domains such as back-arc basins (e.g. Banda Sea), and zones  
 293 undergoing subduction (e.g. west of the Sumatra and Java trenches; east of the Philippines trench); while stage 3  
 294 and 4 seamounts are more common along volcanic arcs (e.g. Banda arc) and intraplate settings (Sunda Shelf, east  
 295 of Vietnam; Fig. 1). An exception is represented by the South China Sea, an intraplate extensional setting, where  
 296 the distribution of all grow stage seamounts is rather uniform, suggesting a more complex interplay of geological  
 297 processes shaping seamount development.

298



299  
 300 **Figure 3. Results of seamount classifications. Seamounts distribution maps based on their morphotype (a) and growth**  
 301 **stage (b) (basemap is from NOAA - DEM Global Mosaic; yellow polygons represent exclusive economic zones).**  
 302 **Distribution plots of water depths (c), and water depths vs morphotypes (d). Distribution of seamount growth stages**  
 303 **(e), and normalised distribution (%) of seamount morphotypes within each growth stage (f).**

304

305 **4.2 Analysis of ‘Exposure Potential’**

306 **4.2.1 Exposure Potential of assets around seamounts (quantitative)**

307 In this section we assess the exposure potential for population, submarine communication cables and ship traffic  
308 within 100 km radius from each seamount (Figures 4 and 5; Fig. S23 and Table S1). We found that 1.3% of the  
309 volcanoes of our catalogue (n= 6) have more than 1M people living within 100 km from them, with Huapingshu  
310 (about 40 km north of Taiwan) exposing about 9.6M people, and two nearby volcanoes (Mienhuayu and  
311 Pengchiahshu) having a similarly high level of exposure (8.2M and 6.8M people), with Taipei lying approximately  
312 60 km away. Krakatau volcano, Indonesia, also ranks high, with nearly 8M people exposed (Fig. 4, Fig. S23),  
313 many in Jakarta, which lies ~140 km to the east. About 8% (n= 39) of the seamounts expose between 100k and  
314 1M people, and these are mostly located within the EEZs of Taiwan, Philippines and Indonesia. There are also a  
315 significant number of seamounts (n= 319) with zero population exposure, mostly located in the central portion of  
316 the northern South China Sea, western Pacific Ocean, and eastern Indian Ocean, and some in the Banda Sea.

317 Exposure for submarine cables has been evaluated in terms of total length of cables within 100 km from each  
318 seamount. About 50% (n= 232) of the seamounts have at least 50 km of submarine cables within their radii, and  
319 approximately 17% of seamounts (n= 78) expose more than 1000 km of cables each. The seamounts with higher  
320 exposure are within the EEZs of Taiwan, Philippines and Vietnam, with Taiwanese volcanoes exposing more than  
321 2500 km of cables each (Fig. 4, Fig. S23).

322 Ship traffic density also shows the highest values around Taiwanese seamounts (Fig. 4, Fig. S23), with the  
323 busiest areas including the Taiwanese strait, western and eastern portions of the northern South China Sea (east  
324 of Vietnam and west of Philippines), Singapore and Malacca Straits, and Gulf of Thailand, with the last three  
325 having zero exposure due to lack of known seamounts nearby. Krakatau also ranks high for ship traffic exposure  
326 (11<sup>th</sup>).

327 In Figure 5, we aggregated exposure to the country level for individual seamount growth stages, and we found  
328 that 5 of the 11 EEZs in the region lie within 100 km of a volcanic seamount (India, Indonesia, Philippines, Taiwan  
329 and Vietnam), in addition to the central portion of the northern South China Sea, which is contended across  
330 different nations (i.e. here referred to as *overlapping claim waters*) and not discussed here. For population, Taiwan  
331 has the highest exposure values (up to nearly 10M people), followed by Indonesia (up to 8M) and the Philippines  
332 (< 1M). For exposure of submarine cables, Taiwan and the Philippines rank the highest (up to >2,000 km of cables  
333 nearby seamounts), followed by Vietnam, and the other EEZs having similar values, with overall less than ~1,500  
334 km of cables within their maritime boarders. For ship traffic density, again, Taiwan reports the highest exposure,  
335 followed by the Philippines, Indonesia, Vietnam and India, with similar values respectively. When considering  
336 the growth stage, besides being the country with the highest exposure values, Taiwan is also the country with  
337 exposure to the seamounts with higher rank (stage 3 and stage 4), and this is shown for all the assets considered.

338

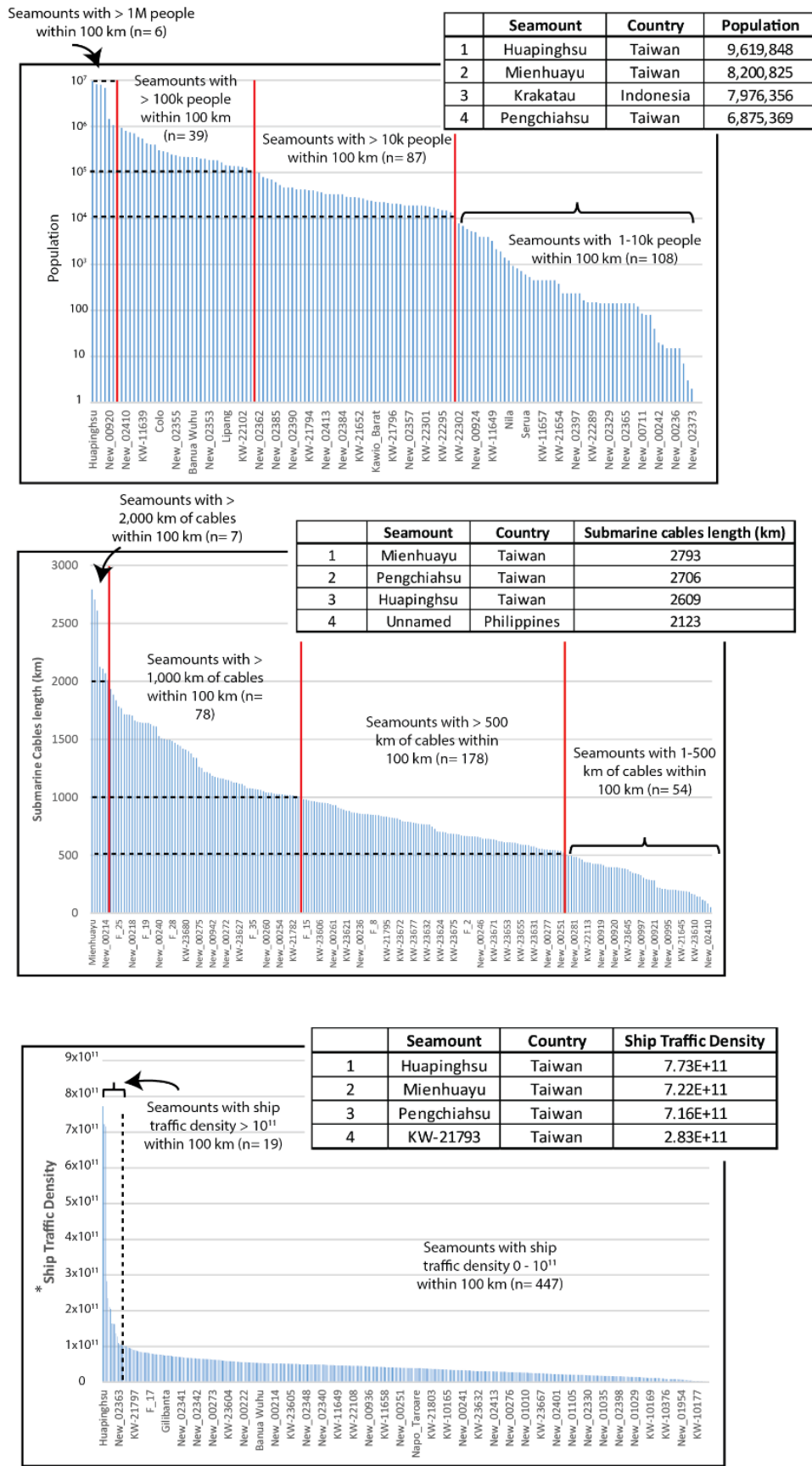
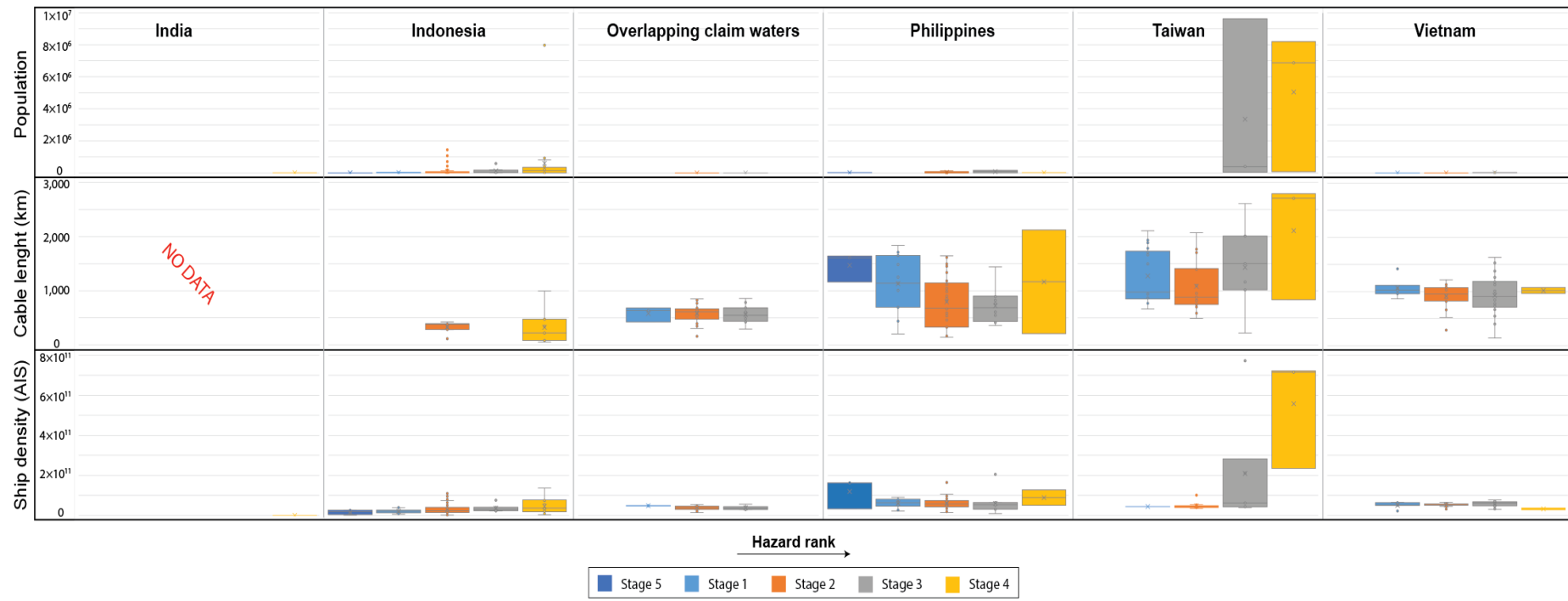


Figure 4. Exposure potential for population (top panel), submarine communication cables (middle panel) and ship traffic density (bottom panel) within 100 km from seamounts in and around SEA. Tables with the top 4 seamounts for exposure are also reported (full seamounts exposure lists are available as additional material; Table S1).



343

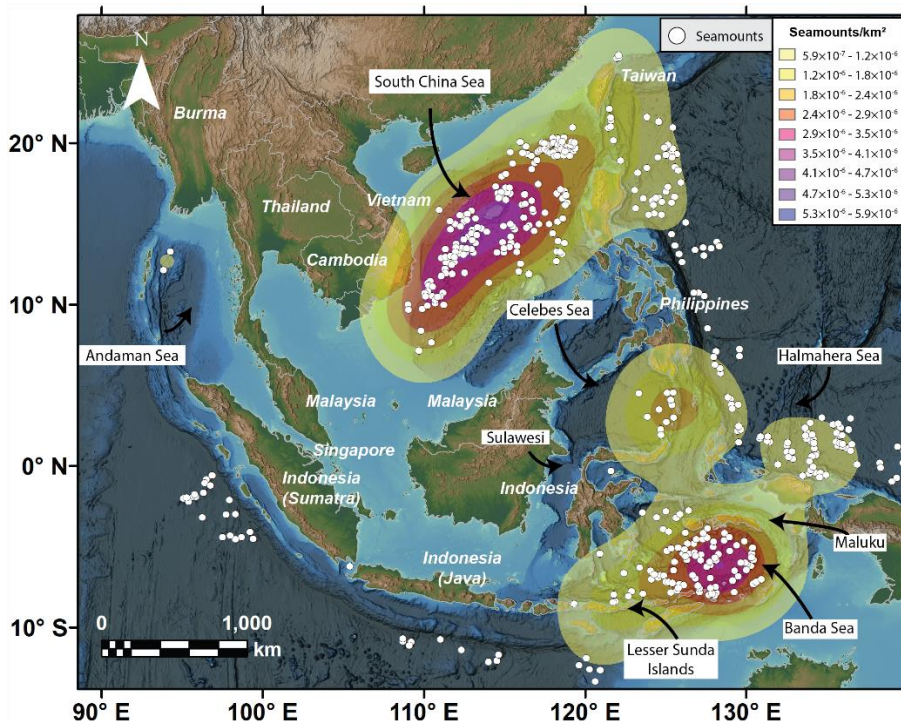
344

345

Figure 5. Exposure potential by country across all stages (ordered from left to right with increasing hazard rank), for population, submarine cables, and ship traffic density. Note that there is no cable data for India's seamounts

346 **4.2.2. Hazard weighted seamount density (semi-quantitative)**

347 We conducted a weighted Kernel Density Estimation (KDE) to understand which regions have higher potential  
348 to produce hazards from a seamount. This estimation is purposely weighted towards the more hazardous  
349 seamounts (Stage 3 and 4) (more details about the weighting process are reported in the methods section). A  
350 sensitivity analysis was run with only stage 3 and 4 seamounts to test the effect of the lower-weighted stage 1, 2  
351 and 5 seamounts, which represent the majority of the seamounts in our study, on the final weighted density map.  
352 Their effect was found to be minor (Fig. S4, Supplementary material), therefore we proceeded with this approach  
353 by including all seamount stages with a given hazard weight (Table 1). The results (Fig. 6) show that there are  
354 two large regions of interest, the largest is in the South China Sea, followed by the Banda Sea. Other areas of  
355 interest, but with lower density, include the Celebes Sea, the Halmahera Sea, and the portion of Pacific Ocean just  
356 east of Taiwan and northern Philippines. Countries surrounding the areas with higher weighted density include  
357 southern Vietnam, southern and northern Philippines, and eastern Indonesia (Sulawesi, Maluku, and Lesser Sunda  
358 Islands).



359  
360 **Figure 6. Hazard-weighted seamount density map in the region of interest. In dark**  
361 **purple the area with higher density of seamounts of higher hazard (see Table 1 for**  
362 **hazard weight).**

363 **5 Discussion**

364 **5.1 Potential sources of volcanic and related hazards in Southeast Asia and its surroundings**

365 Our morphological assessment, while not incorporating geological, absolute age, and frequency/magnitude  
366 data (as further discussed in subsequent sections), offers valuable preliminary insights into the historical and  
367 possible future activities of seamounts. This approach is instrumental in identifying potentially hazardous  
368 seamounts for more detailed investigation in future research, as discussed below.

369 Mienhuayu and Pengchiahstu (offshore north of Taiwan), are two stage 4 simple cones, which lie in waters  
370 shallower than 200 m, with their summits just above sea level (16 and 49 m a.s.l. respectively). We can hypothesise  
371 that simple cones found in shallow waters in our region of interest are likely relatively young, because the sea

372 level rose about 120 m over the last ~20k years (Diekmann et al., 2008; Hanebuth et al., 2011). If volcanoes that  
373 are now in shallow water environments were already existing 20k ago, we could assume that they were at least  
374 partially above water, and this would be reflected in their shape (e.g. presence of prominent terraces on the flanks).  
375 Mienhuayu and Pengchiahsu, which have their base at ~200 m b.s.l., and are considered Pleistocene in Age (100  
376 ka or younger: Global Volcanism Program 2013), would be good case studies to test this hypothesis, however,  
377 the current available resolution prevents us from providing reliable inferences at this stage. Focused bathymetric  
378 and/or seismic surveys around these volcanoes would provide key clues about their relative age (older or younger  
379 than the last glacial maximum, 25 ka). This is important for hazard assessment, because Mienhuayu and  
380 Pengchiahsu are 50-60 km of the Taiwanese mainland and are among the volcanoes that rank the highest in the  
381 quantitative exposure potential analysis for all the assets considered (Fig. 4) (more discussion in the following  
382 sections).

383 The Kawio Barat seamount (~100 km south of the Philippines; Lat: 4.68°, Long: 125.09°) is a large simple  
384 cone rising from about 5,500 m b.s.l. up to ~2000 m b.s.l. (stage 2); it is unlikely that such a high seamount was  
385 formed in a single or short-lived eruptive event. Its regular conical shape, its height and the relatively steep slope  
386 angles (up to >30°) suggest a past explosive or mixed explosive/effusive history, as observed at similar cones on  
387 land; therefore, it represents another candidate to attention for future studies.

388 In this study Krakatau has been classified as a composite and stage 4 seamount, even though it is the newest  
389 cone formed as part of a caldera complex. It is well known for the 2018 eruption collapse-tsunami event (Self,  
390 1992), and for the catastrophic eruption of its predecessor in 1883, which produced PDCs and tsunamis, killing  
391 over 30,000 people (Self, 1992). An example of a less known but still potentially hazardous composite and stage  
392 4 seamount in the region is North Kawio, Indonesia (northern portion of the Sangihe volcanic arc; Lat: 4.68°,  
393 Long: 125.47°). This seamount is reported as Pleistocene in the GVP, but no other information about age is  
394 provided. It is a mostly submerged edifice, with multiple peaks above sea level (e.g. Marore, Kawio, and  
395 Kamboreng islands) and several submarine vents, covering a total area of about 1,500 km<sup>2</sup>. These characteristics  
396 (distributed volcanism), besides the unknown and possibly relatively young age, and the relatively close proximity  
397 to mainland southern Philippines (~100 km south), make North Kawio a potential seamount that could create  
398 tephra and tsunami hazards.

399 In terms of potentially more explosive submarine eruptions, calderas are key morphotypes to consider for the  
400 region. In our classification we identified 4 calderas, 3 of which have their summit at a water depth larger than  
401 ~1,300 m, with 2 of them being deeper than 2,000 m (all stage 2). Some calderas may form due to gradual  
402 subsidence over a longer period of time, hence not associated with any catastrophic explosive event. One key  
403 morphological indicator of either sudden or gradual collapse may be hidden in the intra-caldera slope angles; steep  
404 inner flanks may indicate a sudden sub-vertical movement downward resulting from the magma withdrawal from  
405 a shallow magma chamber. Despite the long-believed concept that explosive volcanic activity is hindered at large  
406 water depths (Cas, 1992), we show in our study that deep calderas with explosive features do exist. Seamount  
407 KW-23612, in the northern South China Sea (Fig. 2c), for example, despite having its rims reaching about 230 m  
408 b.s.l. (stage 3), has the caldera floor at over 2,000 m b.s.l., with inner slope angles up to ~50°. It is unlikely that  
409 such a depression (nearly 2,000 m deep), with such steep caldera walls was formed by gradual subsidence.  
410 Similarly, the recent eruption at the Hunga volcano, was responsible for deepening its caldera floor from an initial  
411 depth of about 200 m to about 850 m (Ribo et al., 2023). The eruption, although initiated at shallow water depth,

412 was responsible for the withdrawal of intra-caldera material up to >800 m through explosive mechanisms, and  
413 this has important implications, once again, about the water depth limit of volcanic explosive eruptions. It is clear  
414 that explosive activity associated with caldera formation can be of rather large magnitude, resulting in high  
415 hazardous scenarios, particularly if this occurs in highly populated areas such as the South China Sea (e.g.  
416 seamounts KW-23612, New-00258) or off the coasts of Indonesia (seamount KW-10401).

417

### 418 **5.13.1 The geodynamic context for SEATANI seamounts**

419 We noted that the geology, absolute age, and eruption frequency/magnitude, were not considered for our hazard-  
420 exposure potential assessment, because of the lack of information for most of the seamounts in the region.  
421 Notwithstanding, in this section we discuss the geodynamic context of the SEATANI seamounts from a regional  
422 perspective, with a particular focus on the two regions that we found to host the highest number of stage 3 and 4,  
423 hence potentially more hazardous, seamounts: the South China Sea and the Banda Sea.

424 There are a~~A~~ number of seamounts (Fig. 6) in proximity~~close~~ to the Indonesian and Philippines trenches that  
425 show zero to very low weighted density, and this reflects their relatively low hazard potential. Seamounts in these  
426 particular tectonic settings are likely millions of years old and no longer active, being at the end of their cycle and  
427 approaching a subduction zone (Staudigel and Clague, 2010). It is likely that also some seamounts in the high  
428 weighted density regions of the South China Sea and Banda Sea may have been extinct for millions of years,  
429 however, these areas represent different~~are in~~tectonic settings, and must be discussed separately.

430 The South China Sea is the result of a multiphase continental rifting and breakup from the Eocene to the  
431 Miocene (e.g. Franke, 2013). Many studies provide evidence for extensive intraplate volcanism in the South China  
432 Sea following the end of the continental rifting (e.g. Xia et al., 2018; Gao et al., 2019; Zhao et al., 2020), with  
433 abundance of Late Cenozoic OIB-type basalts, inferred to be linked to a mantle plume (Yang et al., 2019). A more  
434 recent study identified widespread and partially still ongoing hydrothermal activity in the northern South China  
435 Sea, thought to be associated with magma intrusion (Zhao et al., 2021). On the southwestern edge of the South  
436 China Sea, east of southern Vietnam, there is a submarine volcano that erupted in historical times, Ile des Cendres,  
437 1923. The volcano is located in proximity to a major regional fault, the East Vietnam Fault (Hall and Morley,  
438 2004; Li et al., 2013) (Fig. 1); other major faults exist in the region, Mae Ping Fault and Three Pagodas Fault  
439 (Hall and Morley, 2004; Li et al., 2013), Fig. 1), and others may not be mapped, together with volcanoes in their  
440 proximity. Therefore, despite the intraplate setting, volcanism in the South China Sea may still play a role for  
441 future hazardous scenarios for the region.

442 The Banda Sea, on the other hand, results from more complex~~geodynamics~~. This area was formed by the  
443 initial collision between the Australian and the Banda arc (which was already active from ~12 Ma, (Yang et al.,  
444 2021), and subsequent slab rollback, which created the extensional Banda Sea back-arc basin (Wei et al., 2023).  
445 Therefore, seamounts in this area belong to at least two different formation mechanisms, arc volcanism and back-  
446 arc extensional volcanism. If we consider the seamount growth stage for this area (Fig. 3b), we notice that that  
447 majority of seamounts along the Banda arc are stage 3 and 4, while the seamounts in the central portion of the  
448 Banda Sea basin are stage 2. Most of these stage 2 seamounts are likely as old or older than 3 Ma, given the  
449 inference that volcanism in the Sunda back-arc basin ceased about 3 Ma (Honthaas et al., 1998), however, some  
450 of the~~Banda~~ arc seamounts (i.e. Banda Api, Serua, Nila, and Teon) are reported in the GVP, and erupted in recent  
451 times (within the last ~120 years). Other seamounts are found along this arc and include a stage 3 (New-02400)

452 and a stage 4 (New-02393) seamount. Although we lack geological information from these two volcanoes, their  
453 tectonic setting and proximity to other active seamounts may suggest that they were active in relatively recent  
454 times and may still present a potential threat for the region in case of eruption.

455

## 456 5.2 **Potential Benefit** of multibeam high-resolution image analysis

457 As part of the seamount characterisation, and where multibeam high-resolution (90-m/pixel) bathymetry data  
458 were available, we searched for morphological features on and around seamounts that may give us clues about  
459 past hazards (examples reported in Figure 7). Note that this information is reported here for discussion purposes  
460 only, rather than for quantitative assessment of frequency and type of these past events because multibeam data  
461 only covers < 10% of the region of interest, which may bias the results.

462 We identified several debris avalanche deposits, landslide scars and slumps, explosive craters at depth, new  
463 potential seamounts, and deposits associated with submarine explosive volcanic activity. To understand the  
464 potential of such past hazards, and the impact they would have if they occurred nowadays, we highlight an  
465 example of a large landslide scar and associated deposit near Kawio Barat seamount, in the Celebes Sea, ~100  
466 km south of Mindanao and 90 km north of Sangihe Island, Indonesia (Fig. 7b). We roughly estimated the debris  
467 avalanche volume from the topographic contours (through Esri®ArcMap™ 10.7.1), which resulted in a volume  
468 of ~14 km<sup>3</sup> of material; the deposit includes visible blocks (i.e. hummocks) up to ~500 m in diameter, which are  
469 typical of massive sector collapses (Violante et al., 2003; Idárraga-García and León, 2019; Carter et al., 2020).  
470 For comparison, the sector collapse of Mt Krakatau volcano, Indonesia, in 2018, was about 0.15 km<sup>3</sup>, which  
471 produced a local tsunami with maximum run-up of up to 14 m, and caused over 430 fatalities and millions of USD  
472 damage (Paris et al., 2020 and references therein). The event considered here is likely two orders of magnitude  
473 larger than the Krakatau event, and although the associated potential tsunami hazard cannot be compared directly  
474 because of bathymetric differences at both sites, the size of this event in the Sangihe arc gives us an idea of the  
475 relative scale.

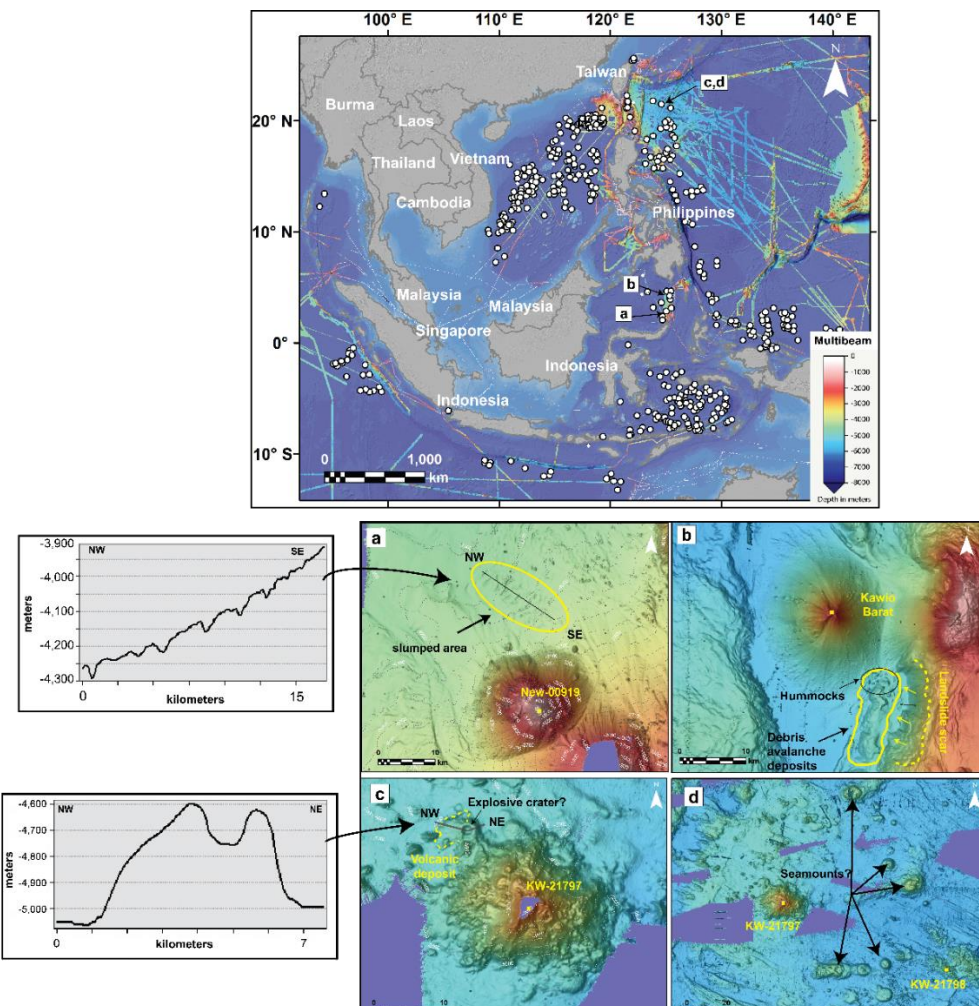
476 Slumps are generally considered less likely to produce significant tsunamis, however, in some instances they  
477 have been inferred as the main cause of devastating tsunamis, such as the 1998 Papua New Guinea event (Okal  
478 and Synolakis, 2003; Brune et al., 2010). Subaqueous slumps appear as transverse ridges with steep toes and block  
479 of various sizes, as have been observed from bathymetric surveys around Hawaii (Moore et al., 1989), and  
480 differently from in contrast to debris avalanches, they are not associated with any amphitheatre-like detachment  
481 area. An example is shown in Fig. 7a, where an area of over 100 km<sup>2</sup> of slumped material is highlighted, just north  
482 of seamount New-00919.

483 Explosive craters provide evidence of volcanic hazards; in Figure 7c we report an example from seamount  
484 KW-21797, ~300 km east-southeast of Taiwan and ~400 km northeast of Luzon, which is a composite and stage  
485 2 seamount, and has a prominent topographic relief with a circular depression at the base of its NW side. This  
486 topographic feature is at a water depth of about 4,600 m, has a crater diameter of approximately 1.5 km and is  
487 around 150 m deep. We interpret this structure as a possible explosive crater because of its relatively large crater  
488 diameter and rather regular circular shape, which may have been formed by an individual explosive event. To the  
489 west of this structure, we identified an apron-like morphology extending westward for about 4 km, which is likely  
490 the volcanic deposit associated with this explosive structure mantling its flank. Though, we cannot rule out the  
491 possibility that this structure and associated deposit may be related to effusive activity forming a westward lava  
492 flow. Evidence of explosive volcanism at water depths  $\geq$  1000 m has been reported in literature, both along

493 volcanic arcs (Murch et al., 2019b), mid-ocean ridges (Sohn et al., 2008), and hotspots (Schipper et al., 2010).  
 494 Additionally, the potential occurrence of explosive deep-sea volcanic eruptions has been proved through analogue  
 495 experiments (Dürig et al., 2020; Newland et al., 2022; Head and Wilson, 2003).

496 In the same area of seamount KW-21797, we identified other possible seamounts (Fig. 7d) that are not reported  
 497 in any official dataset. They are individual composite edifices or chains of composite edifices (at least 3 chains  
 498 can be recognised, all extending along W-E trends). These potential seamounts vary in height from < 500 m to  
 499 ~1500 m, and their summit reaches water depths of ~5,500 to ~4,000 m b.s.l. Although all these seamounts have  
 500 their summit in deep waters, some of them are higher than 1,000 m (stage 2). We do not include them in SEATANI  
 501 as we cannot be sure that they are volcanic, but they may be worth further investigation.

502



503

504 **Figure 7. Map of the study region with multibeam data coverage (top panel), and relevant hazard features**  
 505 **at some of the seamounts investigated, where multibeam data were available (bottom panels, a to d). Two**  
 506 **bathymetric profiles for box a) and c) are also shown.**

507

### 508 **5.3 Potential areas of interest Countries with high hazard/exposure potential**

509 Our seamount characterisation and exposure potential analyses highlights areas potentially more exposed to  
 510 hazards in case of submarine eruption in and around SEA. Taiwan seems to be the candidate that requires more  
 511 attention. It ranks high for both exposure analysis types conducted here. It has the highest number of people  
 512 exposed, with two stage 4 and one stage 3 seamount (the most hazardous types) just 30-60 km northeast of the

513 highly populated Taipei District (>9 M people). A submarine eruption at such distances may affect the nearby  
514 Taiwan through tephra falls and tsunamis. Subaqueous landslides, PDCs, or lava flows can damage the dense  
515 submarine cables array both north and south of Taiwan. Both volcanic and tsunami hazards can affect local ship  
516 traffic, which seems to be the densest in the whole region, with key connection between Taiwan and the rest of  
517 the region through eight major ports.

518 Besides Taiwan, if we consider the exposure by number and type of seamount by country (Fig. 5), Indonesia,  
519 Philippines and Vietnam are potentially threatened too. For Indonesia, the well-known Krakatau volcano is a  
520 hazard for population (~8 M people) and ship traffic, being a key passage to the South China Sea from the southern  
521 Indian Ocean. Eastern Indonesia (Sulawesi, Maluku and Lesser Sunda Island) is mostly exposed to stage 4, stage  
522 3, and stage 2 seamounts. The Philippines is highly exposed as well, with the maximum exposures in the north  
523 (submarine cables, coasts), west (ship traffic) and south (coasts). Vietnam is characterised by high ship traffic  
524 density, with major commercial areas including the Mekong delta and Da Nang port. The Vietnam EEZ encloses  
525 a seamount that erupted in historical time, Ile des Cendres, 1923 (~115 km off the southeast coasts of Vietnam;  
526 Lat: 10.16°, Lon: 109.01). The eruption formed two islands (eroded soon after the eruption and now completely  
527 underwater) and at least another submarine cone (Global Volcanism Program, 2013). There is not much  
528 information about the eruption, but it was thought to be VEI= 2, and a local tsunami along the SE coasts of  
529 mainland Vietnam was also reported (Vu, 2008; Dai Dien, 2010). To our knowledge, there is no detailed study of  
530 the Ile Des Cendres complex, despite it representing the latest episode of submarine volcanism in the region and  
531 having a distributed nature (formation of several vents), which increases the area from which a potential eruption  
532 may occur, hence the hazard.

533 In areas of low seamount density and apparent lower hazard - for example the Indian EEZ (Andaman Sea,  
534 between Sumatra and Burma), which contains just two seamounts, both stage 4 - tsunami can potentially affect  
535 wider areas, such as the coasts of Thailand, Malaysia, Burma, Indonesia (Sumatra), India and, depending on the  
536 magnitude of the event, the coast of Singapore through the Malacca Strait. One of these seamounts is Barren  
537 Island, which shows past evidence of sector collapse (Chandrasekharam et al., 2009). Given the tectonic setting  
538 of these two volcanoes (submarine continuation of the Indonesian volcanic arc), we may expect the presence of  
539 other seamounts in this area not currently charted, hence potential increased hazard extent.

#### 540 **5.3.1 The geodynamic context for SEATANI seamounts**

541 ~~We noted that geology, absolute age, and eruption frequency/magnitude, were not taken into account for our~~  
542 ~~hazard exposure potential assessment, because of the lack of information for most of the seamounts in the region.~~  
543 ~~Notwithstanding, in this section we discuss the geodynamic context of the SEATANI seamounts from a regional~~  
544 ~~perspective, with a particular focus on the two regions that we found to host the highest number of stage 3 and 4,~~  
545 ~~hence potentially more hazardous, seamounts: the South China Sea and the Banda Sea.~~

546 ~~There are a number of seamounts (Fig. 6) in proximity to the Indonesian and Philippines trenches that show~~  
547 ~~zero to very low weighted density, and this reflects their relatively low hazard potential. Seamounts in these~~  
548 ~~particular tectonic settings are likely millions of years old and no longer active, being at the end of their cycle and~~  
549 ~~approaching a subduction zone (Staudigel and Clague, 2010). It is likely that also some seamounts in the high~~  
550 ~~weighted density regions of the South China Sea and Banda Sea may have been extinct for millions of years,~~  
551 ~~however, these areas represent different tectonic settings, and must be discussed separately.~~

552 The South China Sea is the result of a multiphase continental rifting and breakup from the Eocene to the  
553 Miocene (e.g. Franke, 2013). Many studies provide evidence for extensive intraplate volcanism in the South China  
554 Sea following the end of the continental rifting (e.g. Xia et al., 2018; Gao et al., 2019; Zhao et al., 2020), with  
555 abundance of Late Cenozoic OIB type basalts, inferred to be linked to a mantle plume (Yang et al., 2019). A more  
556 recent study identified widespread and partially still ongoing hydrothermal activity in the northern South China  
557 Sea, thought to be associated with magma intrusion (Zhao et al., 2021). On the southwestern edge of the South  
558 China Sea, east of southern Vietnam, there is a submarine volcano that erupted in historical times, Ille des Cendres,  
559 1923. The volcano is located in proximity to a major regional fault, the East Vietnam Fault (Hall and Morley,  
560 2004; Li et al., 2013) (Fig. 1); other major faults exist in the region (Mae Ping Fault and Three Pagodas Fault  
561 (Hall and Morley, 2004; Li et al., 2013), Fig. 1), and others may not be mapped, together with volcanoes in their  
562 proximity. Therefore, despite the intraplate setting, volcanism in the South China Sea may still play a role for  
563 future hazardous scenarios for the region.

564 The Banda Sea, on the other hand, results from more complex dynamics. This area was formed by the initial  
565 collision between the Australian and the Banda arc (which was already active from ~12 Ma, (Yang et al., 2021),  
566 and subsequent slab rollback, which created the extensional Banda Sea backarc basin (Wei et al., 2023). Therefore,  
567 seamounts in this area belong to at least two different formation mechanisms, arc volcanism and backarc  
568 extensional volcanism. If we consider the seamount growth stage for this area (Fig. 3b), we notice that that  
569 majority of seamounts along the Banda arc are stage 3 and 4, while the seamounts in the central portion of the  
570 Banda Sea basin are stage 2. Most of these stage 2 seamounts are likely as old or older than 3 Ma, given the  
571 inference that volcanism in the Sunda backarc basin ceased about 3 Ma (Honthas et al., 1998), however, some  
572 of the Sunda arc seamounts (i.e. Banda Api, Serua, Nila, and Teon) are reported in the GVP, and erupted in recent  
573 times (within the last ~120 years). Other seamounts are found along this arc and include a stage 3 (New 02400)  
574 and a stage 4 (New 02393) seamount. Although we lack geological information from these two volcanoes, their  
575 tectonic setting and proximity to other active seamounts may suggest that they were active in relatively recent  
576 times and may still present a potential threat for the region in case of eruption.

#### 577 5.4 Limitations and future goals

578 A major limitation of this study is the fact that we characterise the hazard potential from seamounts solely based  
579 on morphological (morphotype) and structural information (i.e. water depths, heights), with the high likelihood  
580 of including volcanoes that might have been inactive for millions of years, in turn resulting in an overestimation  
581 of the hazard potential. Despite this, the present study is relevant because it provides the elements to narrow down  
582 the research for future hazard studies from submarine volcanic activity in and around SEA.

583 The choice of the main seamount dataset used for our analysis, that from Gevorgian et al. (2023), was justified  
584 by at least two reasons: (1) it is the most up-to-date seamount dataset in terms of data quality of the Vertical  
585 Gravity Gradient (data noise reduction of 40% from previous VGG datasets; Gevorgian et al., 2023); and (2) it  
586 only focuses on volcanic seamounts, not including small volcanic features such as knolls, which are negligible in  
587 terms of volcanic hazards, and other non-volcanic large features. Even though their method excludes potential  
588 seamounts from within continental margins, potentially biasing our results toward lower hazard potential from  
589 areas such as the Sunda Shelf, we consider it a first approach to be improved upon with higher resolution data.  
590 The use of other global seamount datasets (Cañón-Tapia, 2023, and references therein), which include a higher  
591 number of seamounts (e.g. 33,452 seamounts and 138,412 knolls; Yesson et al., 2011), may have the opposite

593 effect leading to an overestimation of the hazard potential. Future studies should work to integrate the multiple  
594 other seamount datasets, supported by higher resolution bathymetry datasets, when made available, which will  
595 also help to characterise the large number of unclassifiable seamounts (n= 171) from this study.

596 On a parallel note, here we focused on submarine volcanism and excluded large volcanic islands and coastal  
597 volcanoes, however, we acknowledge that similar hazards to those produced by seamounts can be generated by  
598 such volcanoes, and extensive work has been already carried out in SEA (Zorn et al., 2022, and references therein).  
599 Therefore, future work can take advantage of both approaches for a more comprehensive assessment for the  
600 region.

601 The lack of seamounts identified on the Sunda shelf using our method and datasets is a shortcoming of using  
602 the (Gevorgian et al., 2023) dataset that filters out seamounts near continental margins. The known submarine  
603 volcanoes of Ile des Cendres and Veteran, alongside terrestrial volcanoes not reported in this study (e.g. Ly Son  
604 group, Table S2). The general lack of seamounts on the Sunda shelf is questionable. Ile des Cendres and Veteran,  
605 besides other volcanoes not reported in this study because not in line with the definition of seamount used here  
606 (e.g. Ly Son group, Table S2), are in close proximity with a major regional fault, the East Vietnam Fault. Since  
607 this fault extends across the central-eastern portion of the Sunda shelf (all the way south to Borneo inland) (Li et  
608 al., 2013), it would not be surprising to have other volcanoes along or near to this fault zone. Other major faults  
609 mapped on the Sunda shelf include the Wang Chao (Hall and Morley, 2004) and Three Pagodas faults (Li et al.,  
610 2013), but no seamount is known to exist around these areas. The number and type of seamounts potentially not  
611 mapped and not considered for this study, may bias our results, particularly with regards to the KDE assessment.  
612 Potentially, the threat to countries not currently considered exposed, e.g. Singapore, is much greater than currently  
613 appreciated, because of the lack of continental shelf mapped seamounts. However, once again, we emphasize that  
614 here we did not produce any volcanic hazard maps for the region, but rather conducted a simple but  
615 necessary preliminary assessment of hazard and exposure potential, highlighting seamounts and areas of interest  
616 that can be the focus for more-in-depth studies.

617 When it comes to explosive versus effusive behaviour of a given volcano, hence the type of hazards it can  
618 produce, magma composition is a key aspect to consider. In subaerial environments, more silicic magmas are  
619 generally more explosive than basaltic magmas. However, in subaqueous environments the interaction between  
620 external water and magma is often considered the leading trigger of the explosivity of that particular volcano (e.g.  
621 Verolino et al., 2018, 2019). Many pioneer studies on the topic showed that this explosive interaction is more  
622 likely to occur with basaltic magmas (e.g. Wohletz, 1983, 1986; Büttner and Zimanowski, 1998), nevertheless, it  
623 also occurs with more silicic compositions (e.g. Austin-Erickson et al., 2008; Dürig et al., 2020). Magma  
624 composition was not accounted for in our assessment of hazard-exposure potential for two main reasons: 1) Only  
625 GVP seamounts have known composition (despite it could be assumed for some of the seamounts based on their  
626 tectonic setting); And 2) explosivity in subaqueous settings have been observed/inferred across all compositional  
627 domains, hence producing similar hazards regardless of composition. However, one difference is the production  
628 of pumice rafts in silicic eruptions (e.g. Havre, 2012; Fukutoku-Oka-no-Ba, 2021; Carey et al., 2014; Maeno et  
629 al., 2022), which is not expected for basaltic eruptions. Magma composition, eruption dynamics, and  
630 environmental factors that affect hazard extent, distribution and intensity, such as wind conditions or bathymetry,  
631 should be accounted for in future quantitative hazard studies for the region once more information is made  
632 available.

633 Two main issues about the study of seamounts globally and regionally are that 1) the detection from space is  
634 limited within continental margins, and 2) the currently available bathymetry resolution is not enough to allow a  
635 comprehensive morphological characterisation of seamounts. As a result, we end up with large areas without  
636 seamounts (e.g. Sunda shelf), and many unclassified seamounts (n= 171). ~~The general lack of seamounts on the~~  
637 ~~Sunda shelf is questionable. Ile des Cendres and Veteran, besides other volcanoes not reported in this study~~  
638 ~~because not in line with the definition of seamount used here (e.g. Ly Son group, Table S2), are in close proximity~~  
639 ~~with a major regional fault, the East Vietnam Fault. Since this fault extends across the central eastern portion of~~  
640 ~~the Sunda shelf (all the way south to Borneo inland) (Li et al., 2013), it would not be surprising to have other~~  
641 ~~volcanoes along or near to this fault zone. Other major faults mapped on the Sunda shelf include the Wang Chao~~  
642 ~~(Hall and Morley, 2004) and Three Pagodas faults (Li et al., 2013), but no seamount is known to exist around~~  
643 ~~these areas. The number and type of seamounts potentially not mapped and not considered for this study, may~~  
644 ~~bias our results, particularly with regards to the KDE assessment. Potentially, the threat to countries not currently~~  
645 ~~considered exposed, e.g. Singapore, is much greater than currently appreciated, because of the lack of continental~~  
646 ~~shelf mapped seamounts. However, once again, we emphasize that here we did not produce any volcanic hazard~~  
647 ~~maps for the region, but rather conducted a simple but necessary assessment of hazard and exposure potential,~~  
648 ~~highlighting seamounts and areas of interest that can be the focus for more in-depth studies.~~

649 For the quantitative exposure analysis, we used a 100 km radius around each seamount to indicate areas that  
650 may be impacted by volcanic activity. However, concentric radii, despite used in previous hazard studies, are not  
651 a necessarily good approximation of how volcanic hazards behave (Jenkins et al., 2022): some hazards may affect  
652 areas smaller (e.g. lava flows, PDCs) or larger than the 100 km radius (e.g. tephra fall, pumice rafts).

653 Another limitation regards the exact location of submarine communication cables and how many people rely  
654 on this technology. The communication companies provide station to station information, which means that the  
655 exact path of each cable may not be as reported, and this probably partially affects our exposure results.  
656 Additionally, all countries in our study region depend on submarine cables for internet use, which translates into  
657 over 600 million people in the region, however, the cable length analysed here does not give a direct information  
658 on the potential impact from a submarine volcanic eruption, which would be provided, for example, by the exact  
659 number of people that rely on specific cables per country. Despite this limitation, the direct relationship of  
660 seamount and cable density in some areas (northern South China Sea, Luzon Strait, East China Sea) is rather  
661 obvious (Fig. S2) and should be accounted for with regards to future cable installations in the region.

662  
663 The above limitations can be overcome in different ways. One is to improve our collaborative effort with private  
664 and government agencies, which may have seismic and bathymetry data that may improve our understanding of  
665 volcanic hazards from submarine volcanoes in the region. Another is to improve the existing bathymetry datasets,  
666 by combining direct bathymetric information from Gebco and from local nautical charts (Felix et al., 2022); this  
667 will help with a better regional seamount characterisation, hazard assessment, and eventually hazard modelling  
668 and impact analysis at key locations. A third possibility is to use new satellite altimetry data of the sea surface,  
669 which will be made available from NASA in 2024 through the SWOT (Surface Water and Ocean Topography)  
670 mission, which was launched in December 2022. These new data will provide unprecedented resolutions of the  
671 sea surface, which in turn will be used to estimate location of smaller seamount than those currently detectable  
672 from satellite-derived methods, at a global scale. These data could be combined with the bathymetry data for more

673 comprehensive analyses of hazard. Lastly, the results reported in this work, in addition to new data, will provide  
674 an evidence base for more focused investigations to be conducted at potentially high threatening seamounts  
675 (including sampling through Remotely Operated Vehicles, and later laboratory analysis for a complete  
676 characterisation). This will serve countries across the region to become more prepared and resilient against  
677 submarine volcanic hazards.

## 678 **6 Conclusions**

679 Seamounts are an understudied and potentially silent and unseen threat for human populations and infrastructure.  
680 Despite the global identification of about 35,000 seamounts (Gevorgian et al., 2023), only a few of them are  
681 thoroughly studied and monitored (e.g. Deardorff et al., 2011; Caress et al., 2012; Carey et al., 2014; Berthod et  
682 al., 2021). We conducted a seamount characterisation and associated hazard-exposure potential assessment on a  
683 regional scale for SEA and surrounding areas, through the SEATANI dataset, which provides the basis for more  
684 focused investigations of hazards for the region in the future at key locations. Our results show that composite  
685 and stage 2 seamounts are the most abundant in the region, however, stage 3 and stage 4 seamounts (simple,  
686 composite and calderas) are the most important for hazard potential and numbers of people, lengths of cable and  
687 density of shipping exposed. Taiwan has the highest total exposure potential (across all exposure types) within  
688 100 km of volcanic seamounts, followed by Indonesia, Philippines and Vietnam. The hazard-weighted seamount  
689 density assessment highlights two main areas of interest: the northern South China Sea and the Banda Sea. Any  
690 volcanic and related hazards (e.g. tsunamis), if generated in these areas, will potentially affect the coasts of  
691 Southern Taiwan, northern and southern Philippines, Vietnam and eastern Indonesia.

692 This work represents the first step towards understanding the threat that submarine volcanoes pose to  
693 populations and infrastructure in and around SEA. The integration of new bathymetry, seismic and satellite-  
694 derived altimetry data (i.e. SWOT mission) will shed more light on the potential of these volcanoes and enhance  
695 awareness, preparedness and resilience for the countries surrounding these waters.

## 696 **Data availability**

697 Data are available in the supplementary material files and in the public data repository of NTU  
698 (<https://researchdata.ntu.edu.sg/privateurl.xhtml?token=820ea7c9-4ff4-48f8-8e8b-98cd4ffe01f8>)

## 699 **References**

700 Austin-Erickson, A., Büttner, R., Dellino, P., Ort, M. H., and Zimanowski, B.: Phreatomagmatic explosions of  
701 rhyolitic magma: Experimental and field evidence, *J. Geophys. Res.*, 113, B11201,  
702 <https://doi.org/10.1029/2008JB005731>, 2008.

703 Berthod, C., Médard, E., Bachélery, P., Gurioli, L., Di Muro, A., Peltier, A., Komorowski, J.-C., Benbakkar, M.,  
704 Devidal, J.-L., Langlade, J., Besson, P., Boudon, G., Rose-Koga, E., Deplus, C., Le Friant, A., Bickert, M., Nowak, S.,  
705 Thinon, I., Burckel, P., Hidalgo, S., Kaliwoda, M., Jorry, S. J., Fouquet, Y., and Feuillet, N.: The 2018-ongoing  
706 Mayotte submarine eruption: Magma migration imaged by petrological monitoring, *Earth and Planetary Science  
707 Letters*, 571, 117085, <https://doi.org/10.1016/j.epsl.2021.117085>, 2021.

708 Brown, S. K., Sparks, R. S. J., and Jenkins, S. F.: Global distribution of volcanic threat, in: *Global Volcanic Hazards  
709 and Risk*, edited by: Loughlin, S. C., Sparks, S., Brown, S. K., Jenkins, S. F., and Vye-Brown, C., Cambridge  
710 University Press, 359–370, <https://doi.org/10.1017/CBO9781316276273.025>, 2015.

711 Brune, S., Babeyko, A. Y., Gaedicke, C., and Ladage, S.: Hazard assessment of underwater landslide-generated  
712 tsunamis: a case study in the Padang region, Indonesia, *Nat Hazards*, 53, 205–218,  
713 <https://doi.org/10.1007/s11069-009-9424-x>, 2010.

714 Büttner, R. and Zimanowski, B.: Physics of thermohydraulic explosions, *Phys. Rev. E*, 57, 5726–5729,  
715 <https://doi.org/10.1103/PhysRevE.57.5726>, 1998.

716 Cañón-Tapia, E.: Seamount chains and hotspot tracks: Superficially similar, deeply different, *Geoscience*  
717 *Frontiers*, 14, 101659, <https://doi.org/10.1016/j.gsf.2023.101659>, 2023.

718 Caress, D. W., Clague, D. A., Paduan, J. B., Martin, J. F., Dreyer, B. M., Chadwick, W. W., Denny, A., and Kelley, D.  
719 S.: Repeat bathymetric surveys at 1-metre resolution of lava flows erupted at Axial Seamount in April 2011,  
720 *Nature Geosci*, 5, 483–488, <https://doi.org/10.1038/ngeo1496>, 2012.

721 Carey, R. J., Wysoczanski, R., Wunderman, R., and Jutzeler, M.: Discovery of the Largest Historic Silicic Submarine  
722 Eruption, *Eos, Transactions American Geophysical Union*, 95, 157–159, <https://doi.org/10.1002/2014EO190001>,  
723 2014.

724 Carter, G. D. O., Cooper, R., Gafeira, J., Howe, J. A., and Long, D.: Morphology of small-scale submarine mass  
725 movement events across the northwest United Kingdom, *Geomorphology*, 365, 107282,  
726 <https://doi.org/10.1016/j.geomorph.2020.107282>, 2020.

727 Cas, R. A. F.: Submarine volcanism; eruption styles, products, and relevance to understanding the host-rock  
728 successions to volcanic-hosted massive sulfide deposits, *Economic Geology*, 87, 511–541,  
729 <https://doi.org/10.2113/gsecongeo.87.3.511>, 1992.

730 Chadwick, W. W., Cashman, K. V., Embley, R. W., Matsumoto, H., Dziak, R. P., de Ronde, C. E. J., Lau, T. K.,  
731 Deardorff, N. D., and Merle, S. G.: Direct video and hydrophone observations of submarine explosive eruptions  
732 at NW Rota-1 volcano, Mariana arc: SUBMARINE EXPLOSIVE ERUPTIONS AT NW ROTA-1, *J. Geophys. Res.*, 113,  
733 <https://doi.org/10.1029/2007JB005215>, 2008.

734 Chandrasekharam, D., Santo, A. P., Capaccioni, B., Vaselli, O., Alam, M. A., Manetti, P., and Tassi, F.:  
735 Volcanological and petrological evolution of Barren Island (Andaman Sea, Indian Ocean), *Journal of Asian Earth*  
736 *Sciences*, 35, 469–487, <https://doi.org/10.1016/j.jseae.2009.02.010>, 2009.

737 Clague, D. A., Holcomb, R. T., Sinton, J. M., Detrick, R. S., and Torresan, M. E.: Pliocene and Pleistocene alkalic  
738 flood basalts on the seafloor north of the Hawaiian islands, *Earth and Planetary Science Letters*, 98, 175–191,  
739 [https://doi.org/10.1016/0012-821X\(90\)90058-6](https://doi.org/10.1016/0012-821X(90)90058-6), 1990.

740 Clague, D. A., Paduan, J. B., Caress, D. W., Thomas, H., Chadwick Jr., W. W., and Merle, S. G.: Volcanic morphology  
741 of West Mata Volcano, NE Lau Basin, based on high-resolution bathymetry and depth changes, *Geochemistry,*  
742 *Geophysics, Geosystems*, 12, <https://doi.org/10.1029/2011GC003791>, 2011.

743 Clague, D. A., Dreyer, B. M., Paduan, J. B., Martin, J. F., Chadwick, W. W., Caress, D. W., Portner, R. A., Guilderson,  
744 T. P., McGann, M. L., Thomas, H., Butterfield, D. A., and Embley, R. W.: Geologic history of the summit of Axial  
745 Seamount, Juan de Fuca Ridge, *Geochemistry, Geophysics, Geosystems*, 14, 4403–4443,  
746 <https://doi.org/10.1002/ggge.20240>, 2013.

747 Dai Dien, L.: Overview on tsunami risk evaluation and NPP project in Vietnam. 1st Kawashiwazaki International  
748 Symposium on Seismic Safety of Nuclear Installations, 24–26 November 2010, NIIT, Niigata, Japan  
749 ([http://www.nsr.go.jp/archive/jnes/seismic-symposium10/presentationdata/3\\_sessionB/B-09.pdf](http://www.nsr.go.jp/archive/jnes/seismic-symposium10/presentationdata/3_sessionB/B-09.pdf)), 2010.

750 Deardorff, N. D., Cashman, K. V., and Chadwick, W. W.: Observations of eruptive plume dynamics and pyroclastic  
751 deposits from submarine explosive eruptions at NW Rota-1, Mariana arc, *Journal of Volcanology and*  
752 *Geothermal Research*, 202, 47–59, <https://doi.org/10.1016/j.jvolgeores.2011.01.003>, 2011.

753 Diekmann, B., Hofmann, J., Henrich, R., Fütterer, D. K., Röhl, U., and Wei, K.-Y.: Detrital sediment supply in the  
754 southern Okinawa Trough and its relation to sea-level and Kuroshio dynamics during the late Quaternary, *Marine  
755 Geology*, 255, 83–95, <https://doi.org/10.1016/j.margeo.2008.08.001>, 2008.

756 Dürig, T., White, J. D. L., Murch, A. P., Zimanowski, B., Büttner, R., Mele, D., Dellino, P., Carey, R. J., Schmidt, L.  
757 S., and Spitznagel, N.: Deep-sea eruptions boosted by induced fuel–coolant explosions, *Nat. Geosci.*, 13, 498–  
758 503, <https://doi.org/10.1038/s41561-020-0603-4>, 2020.

759 Dziak, R. P., Bohnenstiehl, D. R., Baker, E. T., Matsumoto, H., Caplan-Auerbach, J., Embley, R. W., Merle, S. G.,  
760 Walker, S. L., Lau, T.-K., and Chadwick Jr., W. W.: Long-term explosive degassing and debris flow activity at West  
761 Mata submarine volcano, *Geophysical Research Letters*, 42, 1480–1487,  
762 <https://doi.org/10.1002/2014GL062603>, 2015.

763 Embley, R. W., Chadwick, W. W., Baker, E. T., Butterfield, D. A., Resing, J. A., de Ronde, C. E. J., Tunnicliffe, V.,  
764 Lupton, J. E., Juniper, S. K., Rubin, K. H., Stern, R. J., Lebon, G. T., Nakamura, K., Merle, S. G., Hein, J. R., Wiens,  
765 D. A., and Tamura, Y.: Long-term eruptive activity at a submarine arc volcano, *Nature*, 441, 494–497,  
766 <https://doi.org/10.1038/nature04762>, 2006.

767 Fan, C., Xia, S., Zhao, F., Sun, J., Cao, J., Xu, H., and Wan, K.: New insights into the magmatism in the northern  
768 margin of the South China Sea: Spatial features and volume of intraplate seamounts: INTRAPLATE SEAMOUNTS  
769 IN THE SCS, *Geochem. Geophys. Geosyst.*, 18, 2216–2239, <https://doi.org/10.1002/2016GC006792>, 2017.

770 Felix, R. P., Hubbard, J. A., Bradley, K. E., Lythgoe, K. H., Li, L., and Switzer, A. D.: Tsunami hazard in Lombok and  
771 Bali, Indonesia, due to the Flores back-arc thrust, *Nat. Hazards Earth Syst. Sci.*, 22, 1665–1682,  
772 <https://doi.org/10.5194/nhess-22-1665-2022>, 2022.

773 Feuillet, N., Jorry, S., Crawford, W. C., Deplus, C., Thimon, I., Jacques, E., Saurel, J. M., Lemoine, A., Paquet, F.,  
774 Satriano, C., Aiken, C., Foix, O., Kowalski, P., Laurent, A., Rinnert, E., Cathalot, C., Donval, J.-P., Guyader, V.,  
775 Gaillot, A., Scalabrin, C., Moreira, M., Peltier, A., Beauducel, F., Grandin, R., Ballu, V., Daniel, R., Pelleau, P.,  
776 Gomez, J., Besançon, S., Geli, L., Bernard, P., Bachelery, P., Fouquet, Y., Bertil, D., Lemarchand, A., and Van der  
777 Woerd, J.: Birth of a large volcanic edifice offshore Mayotte via lithosphere-scale dyke intrusion, *Nat. Geosci.*,  
778 14, 787–795, <https://doi.org/10.1038/s41561-021-00809-x>, 2021.

779 Franke, D.: Rifting, lithosphere breakup and volcanism: Comparison of magma-poor and volcanic rifted margins,  
780 *Marine and Petroleum Geology*, 43, 63–87, <https://doi.org/10.1016/j.marpetgeo.2012.11.003>, 2013.

781 Gao, J., Bangs, N., Wu, S., Cai, G., Han, S., Ma, B., Wang, J., Xie, Y., Huang, W., Dong, D., and Wang, D.: Post-  
782 seafloor spreading magmatism and associated magmatic hydrothermal systems in the Xisha uplift region,  
783 northwestern South China Sea, *Basin Res*, 31, 688–708, <https://doi.org/10.1111/bre.12338>, 2019.

784 Gevorgian, J., Sandwell, D. T., Yu, Y., Kim, S., and Wessel, P.: Global Distribution and Morphology of Small  
785 Seamounts, *Earth and Space Science*, 10, e2022EA002331, <https://doi.org/10.1029/2022EA002331>, 2023.

786 Global Volcanism Program: Global Volcanism Program, 2013 (19 June 2021). Venzke, E (ed.). Smithsonian  
787 Institution. Downloaded 19 Jun 2021. <https://volcano.si.edu/volcano.cfm?vn=275813>, 2013.

788 Gusman, A. R., Roger, J., Noble, C., Wang, X., Power, W., and Burbidge, D.: The 2022 Hunga Tonga-Hunga Ha'apai  
789 Volcano Air-Wave Generated Tsunami, *Pure Appl. Geophys.*, 179, 3511–3525, <https://doi.org/10.1007/s00024-022-03154-1>, 2022.

791 Hall, R. and Morley, C. K.: Sundaland basins, in: *Geophysical Monograph Series*, vol. 149, edited by: Clift, P.,  
792 Kuhnt, W., Wang, P., and Hayes, D., American Geophysical Union, Washington, D. C., 55–85,  
793 <https://doi.org/10.1029/149GM04>, 2004.

794 Hammond, S. R.: Relationships between lava types, seafloor morphology, and the occurrence of hydrothermal  
795 venting in the ASHES Vent Field of Axial Volcano, *Journal of Geophysical Research: Solid Earth*, 95, 12875–12893,  
796 <https://doi.org/10.1029/JB095iB08p12875>, 1990.

797 Hamzah, L., Puspito, N. T., and Imamura, F.: Tsunami Catalog and Zones in Indonesia., *Journal of Natural Disaster*  
798 *Science*, 22, 25–43, <https://doi.org/10.2328/jnds.22.25>, 2000.

799 Hanebuth, T. J. J., Voris, H. K., Yokoyama, Y., Saito, Y., and Okuno, J.: Formation and fate of sedimentary  
800 depocentres on Southeast Asia's Sunda Shelf over the past sea-level cycle and biogeographic implications, *Earth-*  
801 *Science Reviews*, 104, 92–110, <https://doi.org/10.1016/j.earscirev.2010.09.006>, 2011.

802 Harders, R., Ranero, C. R., and Weinrebe, W.: Characterization of Submarine Landslide Complexes Offshore Costa  
803 Rica: An Evolutionary Model Related to Seamount Subduction. In S. Krastel et al. (eds.), *Submarine Mass*  
804 *Movements and Their Consequences, Advances in Natural and Technological Hazards Research* 37, DOI  
805 10.1007/978-3-319-00972-8 34, © Springer International Publishing Switzerland 2014, 2014.

806 Head, J. W. and Wilson, L.: Deep submarine pyroclastic eruptions: theory and predicted landforms and deposits,  
807 *Journal of Volcanology and Geothermal Research*, 121, 155–193, [https://doi.org/10.1016/S0377-0273\(02\)00425-0](https://doi.org/10.1016/S0377-0273(02)00425-0), 2003.

809 Hidayat, A., Marfai, M. A., and Hadmoko, D. S.: Eruption on Indonesia's volcanic islands: a review of potential  
810 hazards, fatalities, and management, *IOP Conf. Ser.: Earth Environ. Sci.*, 485, 012061,  
811 <https://doi.org/10.1088/1755-1315/485/1/012061>, 2020.

812 Honthaas, C., Réhault, J.-P., Maury, R. C., Bellon, H., Hémond, C., Malod, J.-A., Cornée, J.-J., Villeneuve, M.,  
813 Cotten, J., Burhanuddin, S., Guillou, H., and Arnaud, N.: A Neogene back-arc origin for the Banda Sea basins:  
814 geochemical and geochronological constraints from the Banda ridges (East Indonesia), *Tectonophysics*, 298,  
815 297–317, [https://doi.org/10.1016/S0040-1951\(98\)00190-5](https://doi.org/10.1016/S0040-1951(98)00190-5), 1998.

816 Idárraga-García, J. and León, H.: Unraveling the Underwater Morphological Features of Roncador Bank,  
817 Archipelago of San Andres, Providencia and Santa Catalina (Colombian Caribbean), *Front. Mar. Sci.*, 6, 77,  
818 <https://doi.org/10.3389/fmars.2019.00077>, 2019.

819 Jenkins, S. F., Biass, S., Williams, G. T., Hayes, J. L., Tenant, E., Yang, Q., Burgos, V., Meredith, E. S., Lerner, G.  
820 A., Syarifuddin, M., and Verolino, A.: Evaluating and ranking Southeast Asia's exposure to explosive volcanic  
821 hazards, *Nat. Hazards Earth Syst. Sci.*, 22, 1233–1265, <https://doi.org/10.5194/nhess-22-1233-2022>, 2022.

822 Jutzeler, M., Marsh, R., Carey, R. J., White, J. D. L., Talling, P. J., and Karlstrom, L.: On the fate of pumice rafts  
823 formed during the 2012 Havre submarine eruption, *Nat Commun*, 5, 3660,  
824 <https://doi.org/10.1038/ncomms4660>, 2014.

825 Kim, S.-S. and Wessel, P.: New global seamount census from altimetry-derived gravity data: New global  
826 seamount census, *Geophysical Journal International*, 186, 615–631, <https://doi.org/10.1111/j.1365-246X.2011.05076.x>, 2011.

828 Li, L., Clift, P. D., and Nguyen, H. T.: The sedimentary, magmatic and tectonic evolution of the southwestern  
829 South China Sea revealed by seismic stratigraphic analysis, *Mar Geophys Res*, 34, 341–365,  
830 <https://doi.org/10.1007/s11001-013-9171-y>, 2013.

831 Moore, J. G., Clague, D. A., Holcomb, R. T., Lipman, P. W., Normark, W. R., and Torresan, M. E.: Proigious  
832 submarine landslides on the Hawaiian Ridge, *Journal of Geophysical Research: Solid Earth*, 94, 17465–17484,  
833 <https://doi.org/10.1029/JB094iB12p17465>, 1989.

834 Murch, A. P., White, J. D. L., and Carey, R. J.: Characteristics and Deposit Stratigraphy of Submarine-Erupted  
835 Silicic Ash, Havre Volcano, Kermadec Arc, New Zealand, *Front. Earth Sci.*, 7, 1,  
836 <https://doi.org/10.3389/feart.2019.00001>, 2019a.

837 Murch, A. P., White, J. D. L., and Carey, R. J.: Unusual fluidal behavior of a silicic magma during fragmentation in  
838 a deep subaqueous eruption, Havre volcano, southwestern Pacific Ocean, *Geology*, 47, 487–490,  
839 <https://doi.org/10.1130/G45657.1>, 2019b.

840 Murch, A. P., Portner, R. A., Rubin, K. H., and Clague, D. A.: Deep-subaqueous implosive volcanism at West Mata  
841 seamount, Tonga, Earth and Planetary Science Letters, 578, 117328,  
842 <https://doi.org/10.1016/j.epsl.2021.117328>, 2022.

843 Mutaqin, B. W., Lavigne, F., Hadmoko, D. S., and Ngalawani, M. N.: Volcanic Eruption-Induced Tsunami in  
844 Indonesia: A Review, IOP Conf. Ser.: Earth Environ. Sci., 256, 012023, <https://doi.org/10.1088/1755-1315/256/1/012023>, 2019.

846 NCEI/WDS: National Geophysical Data Center / World Data Service: NCEI/WDS Global Historical Tsunami  
847 Database. NOAA National Centers for Environmental Information. doi:10.7289/V5PN93H7, n.d.

848 Newland, E. L., Mingotti, N., and Woods, A. W.: Dynamics of deep-submarine volcanic eruptions, Sci Rep, 12,  
849 3276, <https://doi.org/10.1038/s41598-022-07351-9>, 2022.

850 Ohno, Y., Iguchi, A., Ijima, M., Yasumoto, K., and Suzuki, A.: Coastal ecological impacts from pumice rafts, Sci  
851 Rep, 12, 11187, <https://doi.org/10.1038/s41598-022-14614-y>, 2022.

852 Okal, E. A. and Synolakis, C. E.: Field survey and numerical simulations: a theoretical comparison of tsunamis  
853 from dislocations and landslides. Pure Appl Geophys 160:2177–2188, 2003.

854 Omira, R., Ramalho, I., Terrinha, P., Baptista, M. A., Batista, L., and Zitellini, N.: Deep-water seamounts, a  
855 potential source of tsunami generated by landslides? The Hirondelle Seamount, NE Atlantic, Marine Geology,  
856 379, 267–280, <https://doi.org/10.1016/j.margeo.2016.06.010>, 2016.

857 Paris, A., Heinrich, P., Paris, R., and Abadie, S.: The December 22, 2018 Anak Krakatau, Indonesia, Landslide and  
858 Tsunami: Preliminary Modeling Results, Pure Appl. Geophys., 177, 571–590, <https://doi.org/10.1007/s00024-019-02394-y>, 2020.

860 Paris, R., Switzer, A. D., Belousova, M., Belousov, A., Ontowirjo, B., Whelley, P. L., and Ulvrova, M.: Volcanic  
861 tsunami: a review of source mechanisms, past events and hazards in Southeast Asia (Indonesia, Philippines,  
862 Papua New Guinea), Nat Hazards, 70, 447–470, <https://doi.org/10.1007/s11069-013-0822-8>, 2014.

863 Reyes-Hardy, M.-P., Aguilera Barraza, F., Sepúlveda Birke, J. P., Esquivel Cáceres, A., and Inostroza Pizarro, M.:  
864 GIS-based volcanic hazards, vulnerability and risks assessment of the Guallatiri Volcano, Arica y Parinacota  
865 Region, Chile, Journal of South American Earth Sciences, 109, 103262,  
866 <https://doi.org/10.1016/j.jsames.2021.103262>, 2021.

867 Ribo, M., Cronin, S., Stern, S., Park, S. H., Garvin, J., and Kula, T.: Morphological evolution of the Hunga Tonga–  
868 Hunga Ha’apai submarine volcano after the explosive eruption (No. EGU23-17221). Copernicus Meetings., 2023.

869 Schipper, C. I., White, J. D. L., Houghton, B. F., Shimizu, N., and Stewart, R. B.: “Poseidic” explosive eruptions at  
870 Loihi Seamount, Hawaii, Geology, 38, 291–294, <https://doi.org/10.1130/G30351.1>, 2010.

871 Schmidt, R. A. L. F., Schmincke, H. U., and Sigurdsson, H.: Seamounts and island building. Encyclopedia of  
872 volcanoes, 383–402., 2000.

873 Schnur, S. R., Chadwick Jr., W. W., Embley, R. W., Ferrini, V. L., de Ronde, C. E. J., Cashman, K. V., Deardorff, N. D., Merle, S. G., Dziak, R. P., Haxel, J. H., and Matsumoto, H.: A decade of volcanic construction and destruction  
875 at the summit of NW Rota-1 seamount: 2004–2014, Journal of Geophysical Research: Solid Earth, 122, 1558–1584, <https://doi.org/10.1002/2016JB013742>, 2017.

877 Self, S.: Krakatau revisited: The course of events and interpretation of the 1883 eruption, GeoJournal, 28,  
878 <https://doi.org/10.1007/BF00177223>, 1992.

879 Sims, K., Reith, A., Bright, E., McKee, J., and Rose, A.: LandScan Global 2021 [Data set]. Oak Ridge National  
880 Laboratory. <https://doi.org/10.48690/1527702>, 2022.

881 Small, C. and Naumann, T.: The global distribution of human population and recent volcanism, Environmental  
882 Hazards, 3, 93–109, <https://doi.org/10.3763/ehaz.2001.0309>, 2001.

883 Sohn, R. A., Willis, C., Humphris, S., Shank, T. M., Singh, H., Edmonds, H. N., Kunz, C., Hedman, U., Helmke, E.,  
884 Jakuba, M., Liljebladh, B., Linder, J., Murphy, C., Nakamura, K., Sato, T., Schlindwein, V., Stranne, C.,  
885 Tausenfreund, M., Upchurch, L., Winsor, P., Jakobsson, M., and Soule, A.: Explosive volcanism on the ultraslow-  
886 spreading Gakkel ridge, Arctic Ocean, *Nature*, 453, 1236–1238, <https://doi.org/10.1038/nature07075>, 2008.

887 Speidel, U.: The Hunga Tonga Hunga Ha'apai Eruption – A Postmortem: What happened to Tonga's Internet in  
888 January 2022, and what lessons are there to be learned?, in: Proceedings of the 17th Asian Internet Engineering  
889 Conference, AINTEC'22: The 17th Asian Internet Engineering Conference, Hiroshima Japan, 70–78,  
890 <https://doi.org/10.1145/3570748.3570759>, 2022.

891 Staudigel, H. and Clague, D.: The Geological History of Deep-Sea Volcanoes: Biosphere, Hydrosphere, and  
892 Lithosphere Interactions, *Oceanog.*, 23, 58–71, <https://doi.org/10.5670/oceanog.2010.62>, 2010.

893 Staudigel, H., Koppers, A. A. P., Lavelle, W., Pitcher, T. J., and Shank, T. M.: Defining the Word "Seamount," 2010.

894 Taha, G., Loughman, R., Colarco, P. R., Zhu, T., Thomason, L. W., and Jaross, G.: Tracking the 2022 Hunga Tonga-  
895 Hunga Ha'apai Aerosol Cloud in the Upper and Middle Stratosphere Using Space-Based Observations,  
896 *Geophysical Research Letters*, 49, <https://doi.org/10.1029/2022GL100091>, 2022.

897 TeleGeography: Worldwide submarine cables.  
898 <https://services.arcgis.com/6DIQcwIPy8knb6sg/arcgis/rest/services/SubmarineCables/FeatureServer>  
899 (Downloaded on 11 June 2021), n.d.

900 The World Bank: The January 15, 2022 Hunga Tonga-Hunga Ha'apai eruption and tsunami, Tonga Global Rapid  
901 Post Disaster Damage Estimation (Grade) Report.  
902 <https://thedocs.worldbank.org/en/doc/b69af83e486aa652d4232276ad698c7b-0070062022/original/GRADE-Report-Tonga-Volcanic-Eruption.pdf>, 2022.

904 The World Bank Group: Global Shipping Traffic Density.  
905 <https://datacatalog.worldbank.org/search/dataset/0037580>. Downloaded on 13 July 2021., n.d.

906 Verolino, A., White, J. D. L., and Brenna, M.: Eruption dynamics at Pahvant Butte volcano, Utah, western USA: insights from ash-sheet dispersal, grain size, and geochemical data, *Bull Volcanol*, 80, 1–18,  
907 <https://doi.org/10.1007/s00445-018-1256-7>, 2018.

909 Verolino, A., White, J. D. L., Dürig, T., and Cappuccio, F.: Black Point – Pyroclasts of a Surtseyan eruption show  
910 no change during edifice growth to the surface from 100 m water depth, *Journal of Volcanology and Geothermal  
911 Research*, 384, 85–102, <https://doi.org/10.1016/j.jvolgeores.2019.07.013>, 2019.

912 Verolino, A., Jenkins, S. F., Sieh, K., Herrin, J. S., Schonwalder-Angel, D., Sihavong, V., and Oh, J. H.: Assessing  
913 volcanic hazard and exposure to lava flows at remote volcanic fields: a case study from the Bolaven Volcanic  
914 Field, Laos, *J Appl. Volcanol.*, 11, 6, <https://doi.org/10.1186/s13617-022-00116-z>, 2022a.

915 Verolino, A., White, J. D. L., Baxter, R. J. M., Schipper, C. I., and Thordarson, T.: Characteristics of Sub-Aerially  
916 Emplaced Pyroclasts in the Surtsey Eruption Deposits: Implications for Diverse Surtseyan Eruptive Styles,  
917 *Geosciences*, 12, 79, <https://doi.org/10.3390/geosciences12020079>, 2022b.

918 Violante, C., Budillon, F., Esposito, E., Porfido, S., and Vittori, E.: Submerged Hummocky Topographies And  
919 Relations With Landslides. Northwestern Flank Of Ischia Is- Land, Southern Italy, 2003.

920 Vu, T. C.: Earthquake and Tsunami Scenarios in the South China Sea  
921 ([www.ims.nus.edu.sg/Programs/ocean07/files/vu1.ppt](http://www.ims.nus.edu.sg/Programs/ocean07/files/vu1.ppt)), 2008.

922 Wang, Q., Guo, J., Wang, Z., Tahchi, E., Wang, X., Moran, B., and Zukerman, M.: Cost-Effective Path Planning for  
923 Submarine Cable Network Extension, IEEE Access, 7, 61883–61895,  
924 <https://doi.org/10.1109/ACCESS.2019.2915125>, 2019.

925 Wei, X., Luan, X., Meng, F., Lu, Y., He, H., Qiao, J., Yin, J., Wang, Y., and Xue, Y.: Deformation feature and tectonic  
926 model of the Timor Trough: New interpretation of the evolution and mechanism of Banda arc-continent  
927 collision, *Tectonophysics*, 862, 229958, <https://doi.org/10.1016/j.tecto.2023.229958>, 2023.

928 Wessel, P.: Seamount Characteristics. In: Pitcher T, Morato T, et al., editors. *Seamounts: Ecology, Fisheries, &*  
929 *Conservation*. Fish and Aquatic Resources Series 12. Blackwell Publishing., p. 3-20., 2007.

930 Whelley, P. L., Newhall, C. G., and Bradley, K. E.: The frequency of explosive volcanic eruptions in Southeast Asia,  
931 *Bull Volcanol*, 77, 1, <https://doi.org/10.1007/s00445-014-0893-8>, 2015.

932 Wohletz, K. H.: Mechanisms of hydrovolcanic pyroclast formation: Grain-size, scanning electron microscopy, and  
933 experimental studies, 33, 1983.

934 Wohletz, K. H.: Explosive magma-water interactions: Thermodynamics, explosion mechanisms, and field studies,  
935 *Bull Volcanol*, 48, 245–264, <https://doi.org/10.1007/BF01081754>, 1986.

936 Xia, S., Zhao, F., Zhao, D., Fan, C., Wu, S., Mi, L., Sun, J., Cao, J., and Wan, K.: Crustal plumbing system of post-rift  
937 magmatism in the northern margin of South China Sea: New insights from integrated seismology,  
938 *Tectonophysics*, 744, 227–238, <https://doi.org/10.1016/j.tecto.2018.07.002>, 2018.

939 Yang, F., Huang, X.-L., Xu, Y.-G., and He, P.-L.: Plume-ridge interaction in the South China Sea: Thermometric  
940 evidence from Hole U1431E of IODP Expedition 349, *Lithos*, 324–325, 466–478,  
941 <https://doi.org/10.1016/j.lithos.2018.11.031>, 2019.

942 Yang, X., Singh, S. C., and Deighton, I.: The Margin-Oblique Kumawa Strike-Slip Fault in the Banda Forearc, East  
943 Indonesia: Structural Deformation, Tectonic Origin and Geohazard Implication, *Tectonics*, 40,  
944 <https://doi.org/10.1029/2020TC006567>, 2021.

945 Yesson, C., Clark, M. R., Taylor, M. L., and Rogers, A. D.: The global distribution of seamounts based on 30 arc  
946 seconds bathymetry data, *Deep Sea Research Part I: Oceanographic Research Papers*, 58, 442–453,  
947 <https://doi.org/10.1016/j.dsr.2011.02.004>, 2011.

948 Zhao, F., Alves, T. M., Xia, S., Li, W., Wang, L., Mi, L., Wu, S., Cao, J., and Fan, C.: Along-strike segmentation of  
949 the South China Sea margin imposed by inherited pre-rift basement structures, *Earth and Planetary Science  
950 Letters*, 530, 115862, <https://doi.org/10.1016/j.epsl.2019.115862>, 2020.

951 Zhao, F., Berndt, C., Alves, T. M., Xia, S., Li, L., Mi, L., and Fan, C.: Widespread hydrothermal vents and associated  
952 volcanism record prolonged Cenozoic magmatism in the South China Sea, *GSA Bulletin*, 133, 2645–2660,  
953 <https://doi.org/10.1130/B35897.1>, 2021.

954 Zorn, E. U., Orynbaikyzy, A., Plank, S., Babeyko, A., Darmawan, H., Robbany, I. F., and Walter, T. R.: Identification  
955 and ranking of subaerial volcanic tsunami hazard sources in Southeast Asia, *Nat. Hazards Earth Syst. Sci.*, 22,  
956 3083–3104, <https://doi.org/10.5194/nhess-22-3083-2022>, 2022.

957

958 **Acknowledgements**

959 We would like to thank the editor G. Macedonio and the reviewers E. Cañón-Tapia and E. Nicotra for improving  
960 this manuscript. This research was supported by the Earth Observatory of Singapore via its funding from the  
961 National Research Foundation Singapore and the Singapore Ministry of Education under the Research Centers of  
962 Excellence initiative. This work comprises EOS contribution number 531.

963 **Author contribution**

964 AV: Paper conceptualisation and preparation, figures production, data elaboration, analysis,  
965 and interpretation, editing; SFW: data elaboration, analysis,  
966 editing; SJ: paper conceptualisation, editing; FC: paper conceptualisation, editing; ADS: paper conceptualisation, editing.

967 **Competing Interests**

968 We declare no competing interests.